TÉCNICO LISBOA

Implementation of the Prothrombin Time test in the *spinit*® *point of care platform*

Sofia Rodrigues Vaz

Thesis to obtain the Master of Science Degree in

Engineering Physics

Supervisor(s): Doctor João Manuel de Oliveira Garcia da Fonseca
Professor Pedro Miguel Félix Brogueira

Examination Committee

Chairperson: Professor Susana Isabel Pinheiro Cardoso de Freitas
Supervisor: Doctor João Manuel de Oliveira Garcia da Fonseca
Member of the Committee: Professor Pedro José Oliveira Sebastião
Doctor Sandro Miguel Pinto Bordeira

February 2016

Dedicated to my amazing parents and forever younger brother...

Acknowledgments

I am deeply grateful for the opportunity given to me by my supervisor João Fonseca to develop this thesis at *biosurfit*. It was an amazing experience that allowed me to know and work with bright, passionate people who really enjoy every minute of what they are doing, and who made me feel part of the team from the first moment.

I want to thank everyone in the *R&D* team, already my second family, especially Ana Custódio, Lara Borges, Filipe Thomaz, Luís Miguel and Rui Fonseca, for all the time they dedicated to me during my first weeks, and also these last weeks. I also want to thank our *R&D* team leader Nuno Reis for all the enthusiasm and motivation given. João and Nuno definitely set an example for me as great team leaders.

I would also like to thank my family and friends, especially my amazing parents and brother, for all the pep talks, patience and never-ending support over the last years. As for my friends, for those I knew long ago, I am so glad you still are part of my life. And for those I knew only at the university, you were the best part of it all. Adriana Carapucinha, Alberto Ferreira, Ana Sofia Oliveira, Bavieche Samgi, Catarina Torres, Filipe Thomaz, Inês Henriques, José Antunes, Miguel Aleluia, Miguel Prata, Henrique Belo, Madalena Costa, Maria Poiares, Mariana Miranda, Rita Mendes and Sara Martins: You are the best!

Finally, I would like to thank Ana Bela and Pedro Brogueira for all the help they gave me in the final steps of the process.

Thank you all so much!

Resumo

O tempo de protrombina é um ensaio clínico frequentemente usado por especialistas para a detecção de anomalias cardiovasculares, consideradas a maior causa de morte pela Organização Mundial de Saúde.

A análise clínica convencional requer bastante tempo e um tratamento complexo das amostras, estando sujeita a vários erros. Contudo, avanços tecnológicos recentes permitiram o desenvolvimento de pequenos equipamentos automáticos e portáteis, que permitem realizar ensaios clínicos em minutos e com pequenos volumes de amostra, conhecidos como *PoC*.

No trabalho apresentado é feito um estudo que visa a integração do tempo de protrombina na plataforma centrífuga microfluídica *spinit*®, tirando partido do módulo de detecção photoeléctrico que incorpora esta plataforma, e que permite detectar variações ópticas com base em espectrofotometria *PEDD* .

O sinal óptico detectado durante a formação de fibrina foi estudado, e diferentes relações entre o output do *spinit*® e o tempo de protrombina em unidades de índice normalizado internacional (*PT-INR*) foram determinadas.

Diferentes reagentes foram testados, o protocolo de centrifugação foi optimizado, e as definições do sistema óptico usado foram alteradas de forma a permitir encontrar a câmara de detecção o mais rápido possível.

Por último, a qualidade da mistura obtida por diferentes estruturas microfluídicas foi avaliada experimentalmente, usando calibradores de plasma. A estrutura 24 do quarto *layout* testado permitiu obter os melhores resultados, com coeficientes de variação menores que 6% para todos os calibradores, para todas as referências de tempo consideradas.

Palavras-chave: PT-INR, Protrombina, PoC, Hemostase, PEDD

Abstract

The prothrombin time blood assay is used by health specialists in the detection of cardiovascular anomalies, considered the leading cause of death in the world by the World Health Organisation.

Conventional clinical testing is time consuming, requires complex sample handling, and is prone to errors. However, recent technological advances have allowed the development of automatic, small, portable point of care (*PoC*) devices, that operate with small sample volumes, and can give results within minutes.

The present study proposes the integration of the prothrombin time assay in the *spinit*® centrifugal microfluidic platform, taking advantage of its photoelectric detection module, which allows to detect optical changes through paired emitter-detector diode (*PEDD*) based spectrophotometry.

The optical signal variation detected during fibrin formation was studied, and different relations were found between the *spinit*® output and the prothrombin time in international normalised ratio units (*PT-INR*) .

Several reagents were tested, the centrifugation protocol was optimised, and the optical system definitions were changed, in order to find the detection chamber as fast as possible.

Finally, the performance of different microfluidic mixing structures was evaluated experimentally, using plasma calibrators. Structure 24 from the 4th mixing layout tested allowed to obtain the best results, with coefficients of variation lower than 6% for all the calibrators, for all the time references considered.

Keywords: PT-INR, Prothrombin, PoC, Hemostasis, PEDD

Contents

List of Tables

List of Figures

Nomenclature

Greek symbols

μ	Dynamic viscosity $[kg/(ms)]$.
ω	Angular velocity $[rad/s]$.
ρ	Liquid density $[Kg/m^3]$.
σ	Liquid-air surface tension $[N/m]$.
θ	Contact angle.

Roman symbols

D	Diameter $[m]$.
d	Depth $[m]$.
F	Force $[N]$.
f	Force per volume unit $[N/m^3]$.
g	Gravity local acceleration $[m/s^2]$.
l	Linear dimension of the system $[m]$.
P	Pressure $[N/m^2]$.
r	Radius $[m]$.
R_e	Reynolds Number [].
U	Voltage $[V]$.
V	Volume $[m^3]$.
v	Linear velocity $[m/s]$.
w	Width $[m]$.

Glossary

APTT Activated Partial Thromboplastin Time is a medical exam that evaluates the intrinsic path of the coagulation cascade.

CAD Computer-Aided Design

CD Compact Disc

CNC Computer Numerical Control

DVD Digital Video Disc

DVI Digital Visual Interface

INR International Normalised Ratio is the ratio of a patient's prothrombin time to a normal pool of plasma, raised to the power of the ISI value for the analytical system being used.

ISI International Sensitivity Index is an index that indicates how a particular batch of tissue factor compares to an international reference tissue factor.

LED Light Emitting Diode

NIR Near Infra-red

PCI Peripheral Component Interconnect

PC Polycarbonate

PEDD Paired Emitter-Detector Diode

PT Prothrombin Time is a medical exam that evaluates the extrinsic path of the coagulation cascade.

PoC Point of Care

SNR Signal to Noise Ratio

TIR Total Internal Reflection

USB Universal Serial Bus

UV Ultraviolet

WHO World Health Organisation

rpm Rotations per minute

Chapter 1

Introduction

Blood testing has a crucial role worldwide in the detection of health anomalies. It is one of the main resources used by doctors in evaluating one's health status, and the results have a great impact on the health specialist's choice when prescribing the appropriate medication or treatment [1].

In the 60's and early 70's automatic blood chemistry determination began, and it revolutionised the clinical laboratory practice. Blood tests were performed in fixed apparatus of great dimensions operated by highly trained staff. However, not only large quantities of blood were needed, but also the time required to take the tests, the power consumption, as well as the costs associated, were often high [2]. In critical environments such as war zones, places assaulted by natural disasters, or even extraterrestrial platforms, for instance, laboratory facilities are often nonexistent and resources are low. Therefore, the installation of such apparatus might not even be a possibility, no matter how necessary [3].

Typically, blood analysis involves previous separation of interfering cellular components, which is obtained by external centrifugation, followed by manual pipetting of plasma into separate assays. This procedure is both labour and time consuming, taking up to several hours to be completed, which, associated with the separate procedures of sample collection and measurement, makes the whole process impractical and prone to many errors, such as sample misplacement and degradation [1, 2].

1.1 Point of Care Devices

Recent technological advances have allowed the development of small portable devices that were thought of in order to overcome the mentioned disadvantages associated with conventional automatic testing. They are called Point of Care (*PoC*) devices.

These devices have small size and low weight, usually require low power consumption, and also require very small blood samples and reagent volumes, which makes them much more affordable. These characteristics also enable batch-fabrication, so that disposable instruments can be used once and then thrown away, preventing sample contamination. The complexity of the tests performed can vary from simpler procedures to more complex ones, and the results are given within minutes. The fast output is especially important in cases where the patient requires constant monitoring, so that immediate clinical

decisions can be made in case of critical test results. *PoC* devices also tend to be user-friendly, which allows them to be handled not only by healthcare professionals, but in some cases by the patients themselves [4, 3, 5].

1.2 Hemostasis

In 2004 the *World Health Organization* (*WHO*) published a report called *The Global Burden of Disease*, stating that cardiovascular diseases are the leading cause of death in the world, having caused about 32% of all deaths in women and 27% in men in 2004. In developed countries the population has become older and in general is prompted to have more cardiovascular diseases associated with both ageing and as a result of an unhealthy lifestyle, representing one of the most significant causes of death. In low- and middle-income countries, these diseases also occur very frequently, accounting for more than one quarter of the total disease burden in the low- and middle-income countries of Europe. According to the *International Self-Monitoring Association of Oral Anticoagulated Patients*, nearly four million people in Europe take anticoagulants and need to monitor their coagulation time daily [6, 7].

Cardiovascular diseases and other illnesses that eventually lead to surgery are negatively affected by the malfunctioning of the cardiovascular system, and can result in a very serious outcome. The cardiovascular system is mainly responsible for providing with nutrients and oxygen all the cells in our body, as well as collecting carbon dioxide and the waste that results from the cells' activity. It is also responsible for the transportation of enzymes, proteins and hormones, amongst other substances, which makes it of extreme importance [8].

It is essential to guarantee that the cardiovascular system is working properly or, in case of illness, make sure the prescribed medication is correct. In the specific case of patients undergoing cardiac surgery, for instance, the control and adjustment of anticoagulation therapy are essential, in order to avoid accidental bleeding due to abnormal coagulation and/or platelet functions [9].

The human cardiovascular system is composed of a closed network of arteries, veins and capillaries in which blood is propelled by the heart throughout the body [8]. In case of rupture of any of the containing blood vessels, an healthy system is capable of repairing the damage within minutes, avoiding loosing significant quantities of blood and assuring its own subsistence. The combination of all processes that occur in order to seal a site of injury or rupture is called hemostasis. It is the result of mainly three distinct mechanisms intimately related that operate simultaneously: vascular constriction, platelet activity, and the production of stabilised fibrin through coagulation. If any of these mechanisms is excessively active or inappropriately activated, they may result in thrombosis, embolism, or disseminated intravascular coagulation [10].

1.2.1 Coagulation

Coagulation reactions and platelet deposition start immediately after blood is exposed to the subendothelial matrix and extravascular cells. Less than 30 seconds after, fibrin strands start appearing

among the platelets covering the injury site. After several minutes the platelet plug is completely formed and stabilised by fibrin, then the platelets lose their integrity and the plug appears as a mass of fibrin strands only [11]. On the one hand, platelet surfaces have specific receptors crucial to the formation of intermediate and final coagulation proteins known as coagulation factors (*F*), such as fibrinogen, *FV*, and *FVIII*. On the other hand, they can also inhibit coagulation by physically blocking the injury site, lowering the contact between the sub-endothelial proteins that trigger the clot formation and the blood circulating. This reinforces the idea that platelet activity and coagulation are intimately related [10].

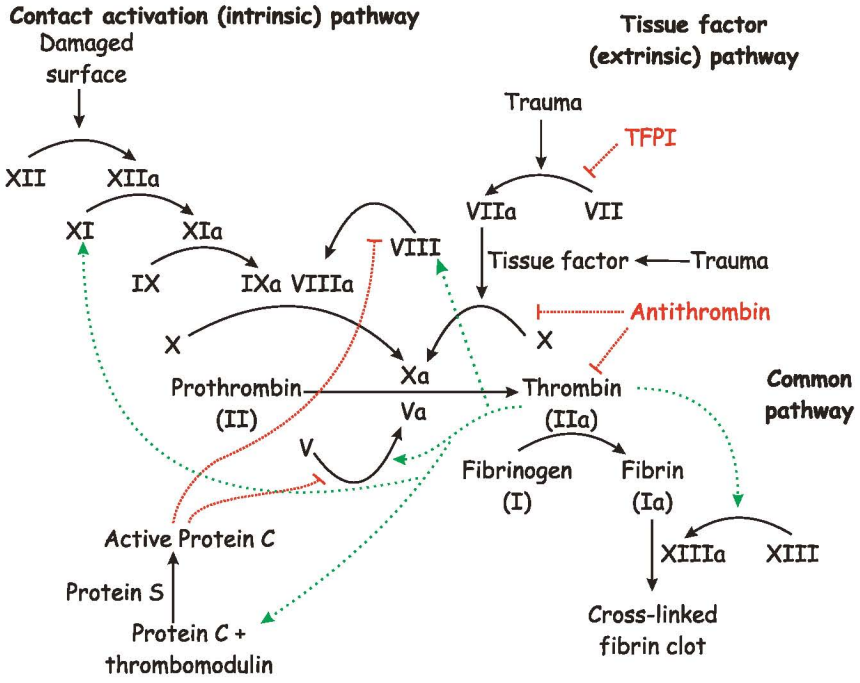

Figure 1.1: Simplified coagulation cascade model, outlined in a Y-shaped scheme with two distinct pathways, intrinsic and extrinsic, that converge into a common pathway. Intrinsic and extrinsic pathways are initiated by the activation of coagulation factors *XII* and *VII*, respectively, triggered by the exposure of blood to collagen and tissue factor, both present in the sub-endothelial matrix [12].

The coagulation model that is still often mentioned was first proposed in the 60s and is called coagulation cascade, as it consists of a sequential series of steps in which the activation of one clotting factor leads to the activation of another, finally leading to fibrin formation [13]. This model is outlined in a Y-shaped scheme with two distinct pathways called intrinsic and extrinsic, initiated by different factors. They will then converge on a common pathway after the activation of factor *V* (*FV* turns into *FVa*). In recent studies, it has been demonstrated that the two pathways do not operate independently as implied by this model [10]. A new cell-based experimental model of coagulation is now being defended [14]. However, it is far more complex and for the purpose of this work the understanding of the older model is enough.

Figure 1.1 shows that the intrinsic and extrinsic pathways are initiated by *F XII* and *FVII*, respectively. The activation of *FXII* occurs in the exposed collagen, present in sub-endothelial tissue. The activation

of *F VII*, on the other hand, occurs in the presence of cell surface receptors called tissue factor (*TF*), also known as *FIII* or thromboplastin [15]. A deficiency in the formation of any of the factors of both pathways may result in a prolongation of coagulation time as the cascade gets partially interrupted.

In spite of the new discoveries made, doctors still evaluate the functioning of each pathway with the results of two main tests, based on the old coagulation scheme: the Activated Partial Thromboplastin Time (*APTT*) and the Prothrombin Time (*PT*) [16]. In fact, in 2011 it was estimated that 800 million *PT* assays are performed annually worldwide [7]. Both tests measure the time it takes to form a thrombus from the instant that a specific reagent is mixed with a blood sample. The main difference consists of the reagents used, that will lead to the activation of the first factor from each path.

The *PT* test evaluates the functioning of the extrinsic and common pathways, through the addition of thromboplastin as a contact activator, as well as calcium chloride. The coagulation times obtained may vary substantially depending on the thromboplastin source used by each laboratory, and also depending on the detection method and equipment used [17]. For these reasons, most laboratories express the results according to the International Normalized Ratio (*INR*), determined by equation 1.1, and in this case the test can be referred to as *PT-INR*.

$$\text{INR} = \left(\frac{\text{PT}_{\text{Lab}}}{\text{Mean Normal PT}} \right)^{\text{ISI}} \tag{1.1}$$

The International Sensitivity Index (*ISI*) is a reference number, usually between 1.0 and 2.0, that compares a particular tissue factor to an *WHO* international standard. Each laboratory assigns a specific *ISI* value for every tissue factor manufactured, assuming it will be used in a specific equipment. Different combinations of reagent-device can change the thromboplastin sensitivity, and a new *ISI* should be determined after system calibration [17].

1.3 Motivation and Objectives

It was stated before that cardiovascular diseases are the leading cause of death in the world, and also that blood testing is one of the main resources used by doctors in the detection of health anomalies. Being able to provide practical, low-cost *PoC* devices that deliver reliable results without the need of specialists and can be used right next to the patient, even in adverse physical circumstances, is of great importance.

The main goal of this thesis is to develop the *PT-INR* test for the microfluidic *PoC* platform *spinit*®, taking advantage of the detection systems already implemented. This platform, developed by *biosurfit, SA*, relies on centrifugal microfluidic and posterior detection through surface plasmon resonance, optical microscopy or photoelectric measurements, for immunoassay, cytology and chemistry assay tests [18].

All the detecting mechanisms are incorporated inside the *spinit*® device, in which disposable discs such as those represented in figure 1.3 are placed, after the capillary blood sample is inserted inside them.

Currently, two types of disposable discs are already available in the market: the *spinit*® *CRP* and the

Figure 1.2: *spinit*® platform [19].

Figure 1.3: Different kinds of *spinit*® discs [18].

spinit® *BC*. The first test is based on a biological recognition layer developed using antibody fragments that can act as selective traps for specific blood markers, and is used to measure C-Reactive Protein concentration in blood, serum and plasma samples, allowing to know the difference between bacterial and viral infections. The second is used to measure and discriminate the total number of Leukocytes, and the percentage of Hematocrit. There are also other discs being developed at the moment: the *spinit*® *inflammation*, the *spinit*® *HbA1c* and the *spinit*® *Lipids* [19].

As was mention before, the *PT-INR* test is extremely important to monitor patients that take anticoagulants, or are having surgery, making it a test often required by doctors. The goal of this work is to develop a reliable low cost *PT-INR* test for the *spinit*® that can be integrated with other tests, which will help improve healthcare quality worldwide.

Chapter 2

Background

2.1 Microfluidics

PoC devices operate with small volumes of reagents and blood samples. Therefore, all the usual sample and reaction processing have to be made at a microlitre scale. On the one hand, this allows the development of separate functional blocks that can be integrated into one, so that different tasks can be performed by the same device, reducing labor and the risk of sample contamination. On the other hand, it is necessary to invest in new fluid propulsion techniques. There are several technologies for moving small fluid and suspended particle volumes. Pressure, acoustic, electrokinetic and centrifuge fluid propulsion are some of the most common mechanisms [5].

The vast majority of biotechnology equipment today is still based on traditional pumping. This approach relies on well-developed, commercially available components, and it allows that a very wide range of flow rates can be attainable. However, these pumps only generate modest flow rates and low pressures, they consume considerable power, and occupy large chip areas [5].

Acoustic propulsion consists of creating a continuous fluid motion induced by an oscillating sound field at a solid or fluid boundary. This method is insensitive to the chemical nature of the fluids inside the channels, and has a promising ability to mix fluids. However, it is not sufficiently developed and can become more expensive [5].

Electrokinetic propulsion does not involve moving parts and is easily implemented. It only needs a metal electrode in a reservoir at each end of a small flow channel. However, it requires a high voltage supply of 1-30kV that will be in direct contact with the fluid, resulting in a sensitivity variation of the system, depending on the charge of the walls and the ionic strength and pH of the solution. Liquids with high ionic strength can cause excessive Joule heating, which is what makes this mechanism inappropriate to pump biological fluids such as blood or urine [5].

Centrifugal pumps, on the other hand, are relatively insensitive to physicochemical properties such as pH, ionic strength, or chemical composition. In fact, blood and urine have already been pumped successfully. It provides a larger range of flow rates than acoustic and electrokinetic systems, from 10nL/s or less to 100$\mu L/s$ or more, depending on the fluid, angular velocity and disc geometry. Valving

can be done using capillary valves, in which capillary forces stop the fluid movement at a channel expansion until a rotationally induced pressure is sufficient to overcome them. Hydrophobic methods can also be used. In this case there is no real physical valve required, which may be considered an advantage in several situations. However, there is no simple way to stop vapours from spreading, which is inconvenient if liquids need to be stored for a long time inside the device [5].

The *spinit*® is a centrifugal microfluidic platform, also known as "Lab-on-CD" platform, and each disc has microfluidic elements integrated that allow reagents resuspension, blood separation, valving, mixing, metering, aliquoting and fluid delivery to the detection areas. The distribution of these elements is made from the centre of the disc to the outer radius, in an order that is related to the order in which the actions need to be performed. The sequence of performed functions rely on different force balances, among which the centrifugal and the capillary forces are very relevant, since they are responsible for moving the fluid away and towards the centre of rotation, respectively [20].

Blood separation is possible as the centrifugal force induced by the disc rotation leads to the deposition of the heavier blood components on the outer walls of a reservoir, due to the difference in their mass density, so that plasma can be collected through the plasma-skimming effect [1].

A fluid on a planar substrate rotating at a distance r from the centre at an angular velocity ω and a linear velocity v with a mass density ρ experiences a centrifugal force (equation 2.1), a Coriolis force (equation 2.2) and an Euler force (equation 2.3), all controlled by the variation of the angular velocity $\omega = \frac{v}{r}$ [20]. The forces can be expressed as follows:

$$\vec{f}_{Centrif}(r) = \frac{\vec{F}_{Centrif}(r)}{V} = \rho \frac{v^2}{r} \vec{e_r} = r\rho\omega^2 \ \vec{e_r}, \tag{2.1}$$

$$\vec{f}_{Coriolis}(r) = -2\rho\omega v \ \vec{e_\theta}, \tag{2.2}$$

$$\vec{f}_{Euler}(r) = -\rho \frac{d\omega}{dt} r \ \vec{e_\theta}. \tag{2.3}$$

Capillary action occurs when liquid molecules adhesion to the walls is stronger than the cohesive forces between them, and it can be quantified as a function of the pressure gradient ΔP that exists at the interface. Equation 2.4 describes the capillary force in a rectangular channel with width w and depth d. σ is the surface tension and θ is the contact angle between the fluid and the channel surface at the interface with air [21, 22]. Considering water our reference fluid, a θ below 90° means the surface is hydrophilic. If θ is higher than 90° then the surface is said to be hydrophobic. Figure 2.1 shows the main forces that act on a disc spinning.

$$\vec{F}_{Cap} = \Delta P w d \ \vec{e_r} = -2\sigma \cos\theta \left(\frac{1}{w} + \frac{1}{d} \right) w d \ \vec{e_r} \tag{2.4}$$

Resuspension and mixing are more challenging functions, and they are essential in order to provide final homogeneous liquid reagents or mixtures that lead to reproducible results. The Reynolds Number R_e is a dimensionless quantity that is used to predict the flow behaviour of a fluid, depending on the

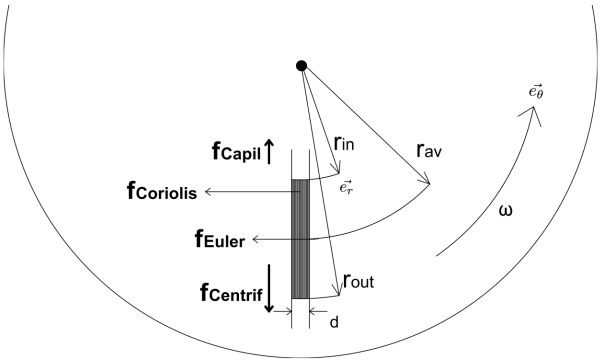

Figure 2.1: Geometry and forces on a disc spinning.

linear dimensions l of the system, the density of the fluid, and also on the dynamic viscosity μ. The relation is expressed by equation 2.5:

$$R_e = \frac{l\rho v}{\mu} \tag{2.5}$$

In the microfluidic scale R_e is well bellow 2300, value that defines the frontier between laminar and turbulent flow, because l and v are both small, whatever the dynamic viscosity happens to be. Therefore, mixing is dominated by diffusion instead of convection, as the flow at this scale is laminar [5].

Diffusion is time-consuming and inefficient in general, especially when the reaction occurs within seconds, as is the case with fibrin formation. In order to overcome this obstacle, several mixing mechanisms have been developed, both active and passive. Active methods require an external energy supply to the system, whereas passive methods take advantage of physical and chemical phenomena such as gravity, capillary action, surface tension or osmosis. An ideal micromixer should have a uniform mixing capability for a wide range of flow rates, but most existing passive micromixers showed relatively good mixing performance only at low flow rates on the micro scale [23]. Various active methods have been proposed for improving the mixing efficiency based on the Coriolis forces, using magnetic beads, spin direction reversal, ultrasounds or even pneumatic agitation. However, despite being more efficient, these methods require rigid constraints and involve a complex fabrication process for both the disc and the centrifugal platform, which makes them financially not viable [1].

In 2014 Ju-Nan Kuo and Bo-Shiun Li proposed a simple *Lab-on-CD* microfluidic platform for achieving rapid mixing of reagents in a seemingly low-cost way that consists on a serpentine structure. This structure links two inner chambers with the fluids that are to be mixed with an outer detection chamber [1]. This idea will be used further on.

2.2 PT Detection Systems Available

Measuring clotting times was, until very recently, a procedure done only by highly trained lab staff. There were two main techniques used, both of them very susceptible to human error and consequent result imprecision: the *tilt-tube method*, which consists in tilting back and forth a tube containing the blood

sample with the reagent, until a visible fibrin clot is formed; and the *wire-loop method*, which consists in passing a wire loop through the mixture of sample and reagent, until the formation and adhesion of a clot to the wire. The time required to perform these tests using conventional bench top systems could take up to 15 minutes, disregarding previous blood separation steps [1]. Nowadays, the new methods that are being developed rely not only on the viscosity changes that occur, but also on other blood properties that also change during coagulation, such as surface tension, electrical conductivity and optical density [7], and can be done within a few minutes only.

There are already some companies that provide *PoC* devices capable of performing the *PT-INR* test. They use different activation reagents and detection methods, being the electrochemical and mechanical methods the most common [24]. Table 2.1 summarises the main characteristics of commercially available *PoC* devices.

Company	Device	Detection Method	Sample (μl)	PT-INR Range	Time (min)
Abbott	i-Stat	Electrochemical	8	[0.9-6.0]	3
Alere	INRatio™	Electrochemical	15	[0.7-7.0]	1
Coag Sense	Coag-Sense™	Mechanical	10	[0.8-8.0]	1
Roche Diagnostics	CoaguChek ®	Electrochemical	8	[0.8-8.0]	1
MicroPoint	qLabs ®	Electrochemical	10	-	2
Helena	Cascade ®	Mechanical	35	-	-
Zafena AB	Simple Simon®PT	Optical	10	[0.7-8.0]	1
ITC	Pro Time®	Mechanical	25	[0.8-9.9]	5

Table 2.1: Summary of the detection methods used by well-known companies for the *PT-INR* test. The information was obtained in each company official website.

As is shown in table 2.1, most *PoC* devices use mechanical or electrochemical detection systems to determine the *PT-INR*. These methods, compared to optical ones and regarding coagulation tests specifically, have been studied for longer and more thoroughly. In fact, optical detection requires a more efficient sample treatment to guarantee that the plasma used in every test is in similar conditions, instead of using whole blood, which has different hematocrit concentrations depending on the person whose it is from. This is important because it has been shown that the coagulation time increases with a decrease in the hematocrit concentration as the interactions among fibrin strands are weakened with this reduction [1]. Also, optical detection requires reagents that are not too opaque, which does not happen with most of the commercially available thromboplastin solutions, made for common automatic mechanical detection apparatus.

Nevertheless, optical detection is a possibility and it is very promising, especially in cases where a microfluidic sample separation can be done, as is the case with the *spinit*® system. An increase in coagulation time is also good for a microfluidic system because stoping rotation and finding detection cameras takes time. Furthermore, in this case it can allow that different tests are performed simultaneously.

2.3 Total Internal Reflection and Paired Emitter-Detector Diode based Spectrophotometry

The *spinit*® photoelectric detection module relies on the concepts of Total Internal Reflection (*TIR*) and also Paired Emitter-Detector Diode (*PEDD*) based Spectrophotometry. This module was first designed to perform colorimetric assays, in order to determine, both directly and indirectly, the concentration of specific coloured compounds in solution. The wavelength λ chosen for the assay should be the closest possible to the one that is absorbed the most by the coloured compound, and in some cases a range of wavelengths can be used. A brief study of the absorption spectrum of the compounds that intervene in a specific reaction can become very useful when trying to understand the final results. Also, the colour of the absorbed λ is not the same as the compound colour.

Spectrophotometry is based on reading the amount of light that passes through a certain solution. The ratio between the incident intensity I_0 and the final intensity I of the light beam with a specific λ, also known as absorbance A, can be related to the properties of the material through which the light is traveling, such as the initial concentration c of the coloured substance, the molar extinction coefficient ϵ, and the optical path length l_{abs}, according to the Beer-Lambert Law (equation 2.6) [25].

$$A = \log\left(\frac{I_0}{I}\right) = \ln(10)\ \epsilon(\lambda)\ c\ l_{abs} \tag{2.6}$$

A coagulation assay can be done using the same detection module. In this case there will be an intensity I decrease throughout time as fibrin is formed, because the sample becomes increasingly more viscous, leading to an increase in the refractive index of the medium and a consequent increase in light scattering, rather than absorption. The angle of measurement and the optical path lengths affect the final results [26]. The Beer-Lambert Law does not specify what causes the light intensity decrease, which can occur due to absorption, scattering and/or reflection. However, the right member of equation 2.6 is useful only when the light intensity decreases due to mainly one attenuation factor.

One of the challenges of the module inside the *spinit*® was finding a way to increase the optical path. A direct emission and further detection of light perpendicular to a disc that is 1.2mm thick, with detection chambers that are only 0.2mm thick would only allow to obtain signals at least 5 times smaller than the ones obtained with typical absorbance and turbidimetric detection systems that use cuvettes with an optical path of 1cm. This limitation would originate a system with poor resolution and precision. Meanwhile several approaches such as optical waveguides or integrated micro-lenses have been tested, although they require complex chip designs and high-accuracy alignment of the optical components that increase the cost of the detecting system [27].

My colleague Filipe Thomaz first tackled this issue, as part of his Master's Thesis in 2014 [27], and alongside other colleagues from *biosurfit* has developed a system in which a Light Emitting Diode (*LED*) emits light that is deflected $90°$ when it reaches the disc via *TIR*, so that it can travel parallel to the disc surface through the detection chamber. After travelling through the full length of the chamber the light is reflected $90°$ again, in order to be detected by another *LED* operating in reverse mode. Similar

geometries have already been used on other centrifugal microfluidic platforms for *POC* testing [27, 25]. Figure 2.2 represents the detection geometry.

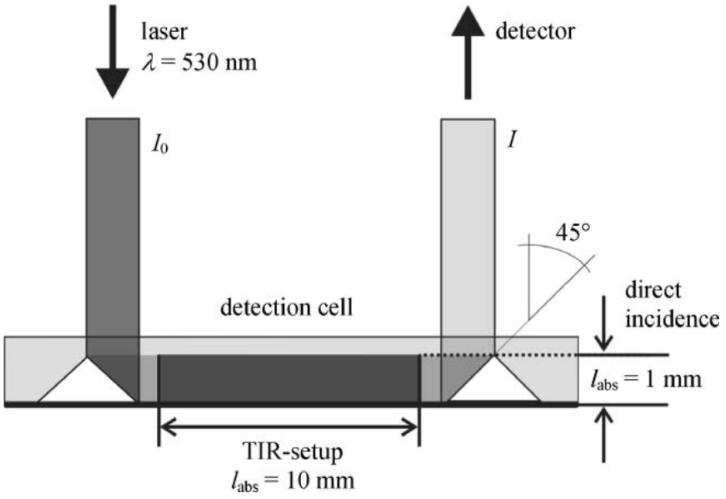

Figure 2.2: Optical light guidance by *TIR* at triangular prisms inclined 45° at the rear side of the surface. The values shown are the ones used in the experiment described in the article [25], source of the figure.

When light travels from a medium with refractive index n_1 to another medium with a higher refractive index n_2, according to the Snell's Law the critical angle α_c above which all the light is reflected is determined as follows in equation 2.7. To ensure *TIR*, the angle of incidence has to exceed the critical angle [25, 27].

$$\alpha_c = \sin^{-1} \frac{n_1}{n_2}. \tag{2.7}$$

Several polymers often used in clinical diagnostics have a refractive index $n_2 \simeq 1.5$. If the light travels from air with a refractive index $n_1 \simeq 1$ to these polymers, the critical angle given by equation 2.7 is approximately $41°$. Then, a structure like a triangular prism with a surface deviated 45° from the horizontal interface surface can deflect all the light emitted perpendicularly to the disc surface that reaches the prism. Light will then travel horizontally through the chamber along a new increased optical path, until it reaches a similar symmetric structure on the opposite side and is deflected 90° again, until it reaches a final detector perpendicularly to the interface [25, 27].

Light Emitting Diodes were first chosen to be used both as light emitters and detectors in the *spinit*® because they are significantly cheaper than photodetectors and photodiodes and are easily available. In fact, *LED*s are currently widely used in modern photoelectronics, because they are considered small, stable and robust low-powered light sources with a long lifetime expectancy. They cover a broad spectral range from ultraviolet (*UV*) to near infrared (*NIR*) wavelengths, at the same time having a narrow emission spectra [28, 29, 30].

A *PEDD* device consists of two light emitting diodes, in which one works as the light source and the other, operating in reverse mode, works as the light detector. The current-voltage characteristic of diodes in either forward or reverse mode is described by the Shockley Ideal Diode Equation (2.8), where

i is the diode current, i_S is the saturation current, *U* is the voltage across the diode and $U_T = \frac{kT}{q}$ is the thermal voltage. The thermal voltage depends on the Boltzmann's constant k, the absolute p-n junction temperature T and the elementary charge q [28, 31, 29].

$$i = i_S \left[e^{-\frac{U}{U_T}} - 1 \right] \simeq i = i_S e^{-\frac{U}{U_T}}, \tag{2.8}$$

The light intensity illuminating the detector-*LED*, I_L, is directly proportional to the current supplying the *LED*-emitter, I_C, so the exponential Shockley Equation 2.8 can be rewritten in the logarithmic form 2.9, where a and b are constants [28]:

$$U = a + b \log I_C = a + b \log I_L. \tag{2.9}$$

If the maximum light intensity $I_L = I_{max}$ is emitted directly into the detector, without travelling through a medium that can absorb or scatter light (the air can be considered such a medium), the detector will measure a corresponding maximum voltage U_{max}, assuming it is smaller than the saturation limit U_{sat}. If light is emitted towards a sample (I_{sample}) and only then reaches the detector, the corresponding detection voltage U_{sample} will be smaller than U_{max}, and its value will vary depending on the characteristics of the sample (equation 2.10) [28]:

$$U_{sample} = a + b \log I_{sample}. \tag{2.10}$$

Thus, the voltage difference measured by a *PEDD* device for a particular sample is directly proportional to the logarithm of the transmitted intensity (equation 2.11), and b represents the system sensitivity [28]:

$$\Delta U_{sample} = U_{max} - U_{sample} = b \log \left(\frac{I_{max}}{I_{sample}} \right) \tag{2.11}$$

Transmission loss can be due to both absorption and/or scattering, depending on the sample's characteristics. As mentioned before, if absorption is the most relevant cause of intensity loss, then the Beer-Lambert Law can be used to determine the sample's initial concentration. However, for the *PT-INR* test specifically the sample becomes increasingly viscous, and therefore scattering plays a major role.

LED-photodiodes are considerably less sensitive than commercially available photodiodes, which makes the traditional direct measurement of the photocurrent more difficult. In order to overcome this issue, in 2005 a Mitsubishi team developed a way of making very precise and accurate measurements of the photocurrent, using a simple threshold detector and a timer circuit. The idea is that a light detector-*LED* reverse biased to an initial voltage U_0 is discharged by the photocurrent i_{light} generated by the incoming light, until it reaches a lower threshold voltage U_t at an unitary discharge instant t_d. This method is said to achieve a great sensitivity and signal-to-noise ratio (*SNR*) in comparison to other methods. The total discharge time t for the *LED* equivalent circuit can be described by equation 2.12, where Q is the accumulated charge and i_{dis} is a small current escape that is usually insignificant compared to i_{light} [32]:

$$t = \frac{Q}{t_{dis} + i_{light}} \simeq \frac{Q}{i_{light}}. \tag{2.12}$$

The electric charge is a constant, therefore, t is inversely proportional to the intensity of the detected light [32]. Figure 2.3 shows the relation between detected voltages and the corresponding discharge times.

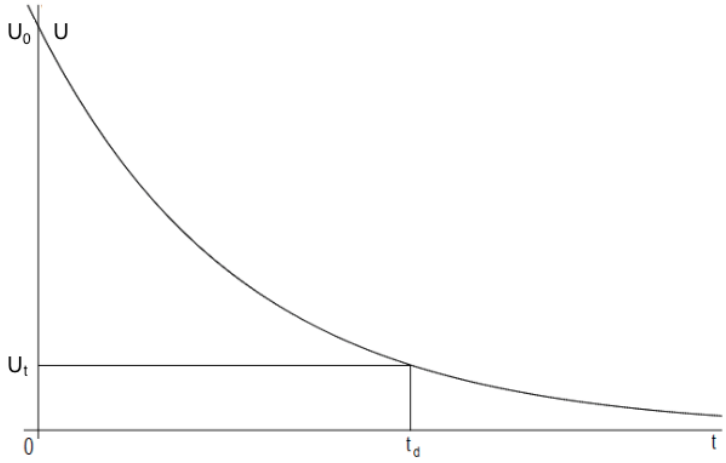

Figure 2.3: Discharge times of the *LED* used as detector, charged initially at a voltage U_0. The threshold voltage U_t occurs at the discharge time t_d.

Chapter 3

Implementation

3.1 Experimental Setup

In this section all the materials used are described, from the *spinit*® and its detection system, to the discs that incorporate microfluidic elements.

3.1.1 *spinit*®

Two *spinit*®s were used in the experiments, both were fitted with an optical module, and one of them allowed to fix the temperature. Fig.3.1 shows one of the two *spinit*®s used.

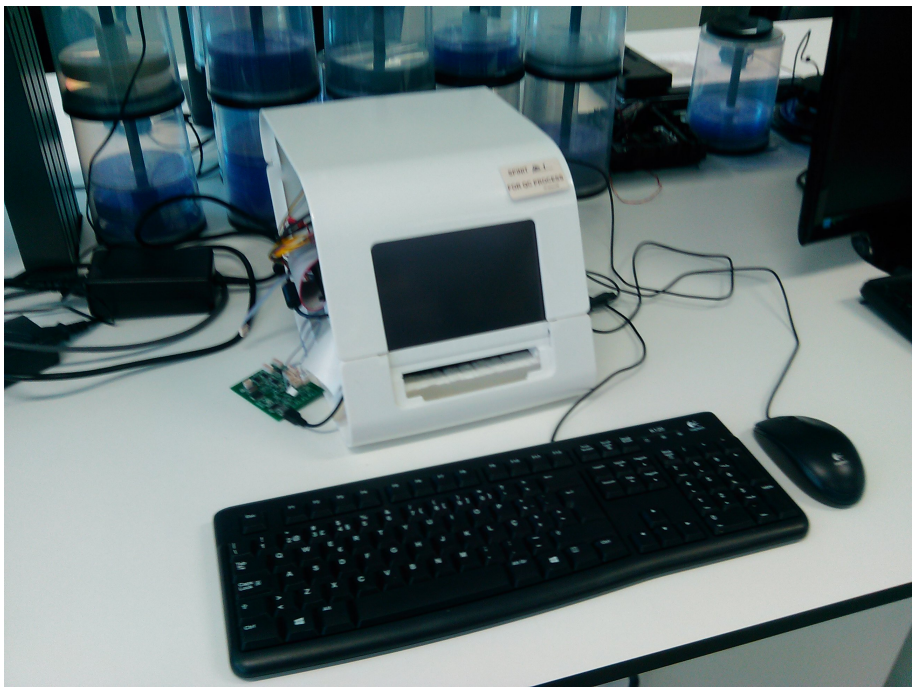

Figure 3.1: One of the two *spinit*®s used in the experiments.

A *spinit*® runs the *Ubuntu* operating system. It has a stepper motor connected via *USB* to the motherboard for positioning the discs, and a screen connected by *DVI*. It also has a regular disc drive

inside for spinning discs at high frequencies, connected to the motherboard via *PCI*. Depending on the input commands given, the disc drive can perform several actions, including eject, inject, start and stop rotation, reaching a defined speed, rotate clockwise or counterclockwise, etc.

Electric Board

The electric board that controls the *LED*s' functions was designed specifically for the *spinit*® and is a result of an optimisation process in order to allow detection of saturation discharge times (*DT*) up to 65000DT_0 (33280μs) when measured in complete darkness, for the 605nm *LED*. DT_0 = 0.512μs will be the representation of the elementary discharge time unit from now on. The saturation discharge times may change depending on the emitter characteristics, such as its wavelength or maximum intensity.

The board has several *LED* sockets from which half are intended to be used as emitters and the other half as detectors. Its baud rate is 38400Hz. It uses a conventional microprocessor incorporated with an internal clock to measure the *LED*s' discharge times. The output is given as a function of the internal clock unit.

The board also has another microchip with drivers installed in order to allow the *USB* to function as a Serial port. This enables communication between the board and the computer, allowing to send commands to each *LED* socket such as voltage settings to turn the *LED*s ON and OFF, clear previous commands, setting the threshold voltage U_t = 1.7V, etc.

LEDs and Detection Chambers

The *LED*s' setup used was already implemented inside each *spinit*®, below the disc drives. It consists of an orange emitter *LED* with λ = 605nm and half-viewing angle of 4° (angle at which the light emitted has half of the intensity of the light emitted forward). The detector, which was initially a 625nm *LED* with a half-viewing angle of 8°, is now an infrared photodiode *LED*.

The distance between the emitter and detector in the device is fixed, in order to assure that the light that reaches the detector without a sample is always the same, so that different tests performed at different times can be compared to each other. A good alignment is essential. The amount of light reaching the detector can still be altered, in a controlled way, by varying the current or tension applied to the emitter *LED*.

3.1.2 Discs

Different disc constructions and layouts were used throughout the experiment. Changes in the layouts directly reflected the purpose of the study, whereas construction changes occurred mostly in order to keep up with parallel research being made at *biosurfit*. The final goal of this work is to develop an assay that can eventually be incorporated with other assays also being developed at *biosurfit* at the moment, which is why trying to use the same materials and construction scheme is so important.

The *spinit*® works with discs that are 1.2mm thick. These discs can be composed of two 0.6mm bonded disc halves, or a single 1.2mm thick disc. Either way, an assembly process is required, and it

varies depending on the materials used. In the first case, it is necessary to bond the two disc halves into one single piece, and in the second case it is necessary to seal the single 1.2mm disc. In this work two different constructions were used.

The first construction consisted of two polycarbonate half discs with a thickness of 0.6mm and a radius of 60mm, bonded with a hydrophilic film. Polycarbonate is the standard optical media used nowadays (*CD/DVD*s), which makes it cheap and available. However, it is a hydrophobic material, which requires the use of additional hydrophilic films or coatings. One half disc has the chambers for both the reagent and the sample, as well as the microfluidic mixing structures. The other half disc has the detection chambers and reflective structures, shown in fig.3.2. *TIR* takes place inside the disc that contains the detection chambers and reflective structures on each side of the optical path. These reflective structures have the shape of triangular prisms, with walls making 45° from the horizontal surface above, and a height of 200μm, the same as the detection chambers depth.

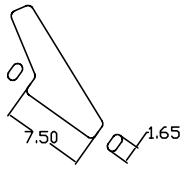

Figure 3.2: Chamber layout with dimensions measured in mm. The optical path is 7.5mm.

The shape of the detection chambers was designed as a function of the position occupied by the *LED*s inside one of the *spinit*®s. The optical path is on the outer side of the chamber, so that centrifugation fills all the optical path with a defined volume, and the remaining volume stays in the inner side of the chamber. Ideally, these walls should be completely perpendicular to the disc surface, in order to guarantee that all the light reflected in the prisms goes inside the chamber without losses due to unwanted reflection. In reality, there is a small deviation angle of about 2° due to manufacture. The disc halves with detection chambers have six chambers with an optical path of 7.5mm, 24° apart from each other, and are manufactured by *Axxicon*, by injection moulding. The layout of the disc with six detection chambers is shown in fig.3.3.

The second construction used consisted of a 1.2mm thick *PC* disc, with a 60mm radius and a completely new layout. This new disc contains both the prisms and detection chambers, but they are very different from the ones used in the first construction. This required the use of a different *spinit*® with the *LED*s setup in a different position.

The new prism discs have twenty four detection chambers, twelve of which with a 10mm optical path and the other twelve with a 7.5mm optical path. The layout of these discs is shown in fig.3.4. The twenty four chamber discs are also manufactured by *Axxicon*, using a slightly different technique that allows the new prisms to be much more polished, with a smaller deviation angle from the ideal 90°. The new layout was thought of in order to make use of the whole disc, allowing to perform up to twenty four tests in a single disc. Also, the necessary volume to fill in the detection chambers is slightly smaller than the volume needed for the six prism discs. The same mould can be used to make discs with different

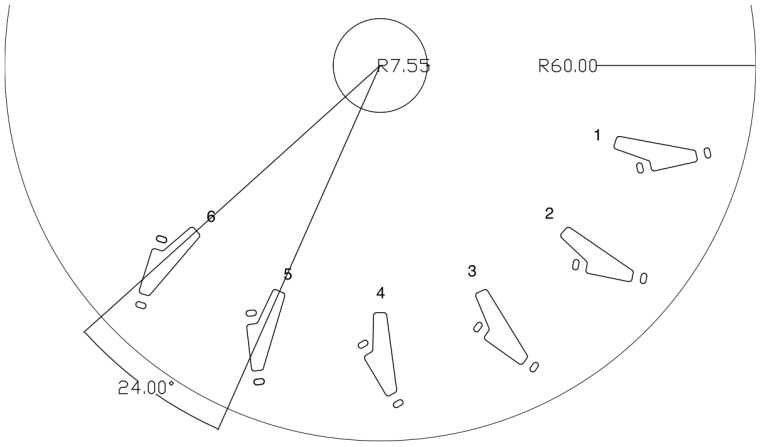

Figure 3.3: Layout of disc with six detection chambers. All six chambers are numbered in the order they will be called from now on, separated 24° from each other.

thicknesses.

The 1.2mm discs were bonded with a *PC* thin layer on top. These discs are manufactured using the exact same mould as similar 0.6mm thick twenty four chamber discs. The only difference is the extra 0.6mm thickness of the disc, which does not affect the depth of the detection chambers, nor the prisms. However, it means that light has to travel through an extra distance of 0.6+0.6mm before reaching the detector. In this case the mixing structures and inlet chambers were milled directly on the prism discs.

Control Milling Cutter

The disc halves with microfluidic structures are initially plain discs that are milled with a computer numeric control milling cutter (*CNC*) at *biosurfit*. This machine is controlled via the software *MACH* and allows precise movement within acceptable tolerance. The perforation is made with a cutting miller in a rotating platform fixed in the apparatus. Fig.3.5 shows the milling cutter on the left side, the motor control in the centre and the milling cutter control on the right.

Several layouts with different mixing structures were designed and tested. They all consisted of two chambers, one for the reagent and the other for the sample, a mixing path, an air vent and through holes.

During each test the chamber's holes were sealed with duct tape, and during centrifugation the air inside the detection chamber leaves through the air vent, as the chamber is filled with the mixture.

The microfluidic layouts were designed using a standard *CAD* software, and were then transferred to a final ".tap" file using a software that transforms the drawings into a set of sequential coordinates that will be sent to *MACH* and eventually covered by the machine.

Assembly Process

For the discs bonded with the hydrophilic film this process was done in a room with controlled temperature and humidity, and UV free, necessary conditions as the film is sensitive to them. The film was first placed on top of the disc with the detection chambers and thermo-laminated at moderate temperature.

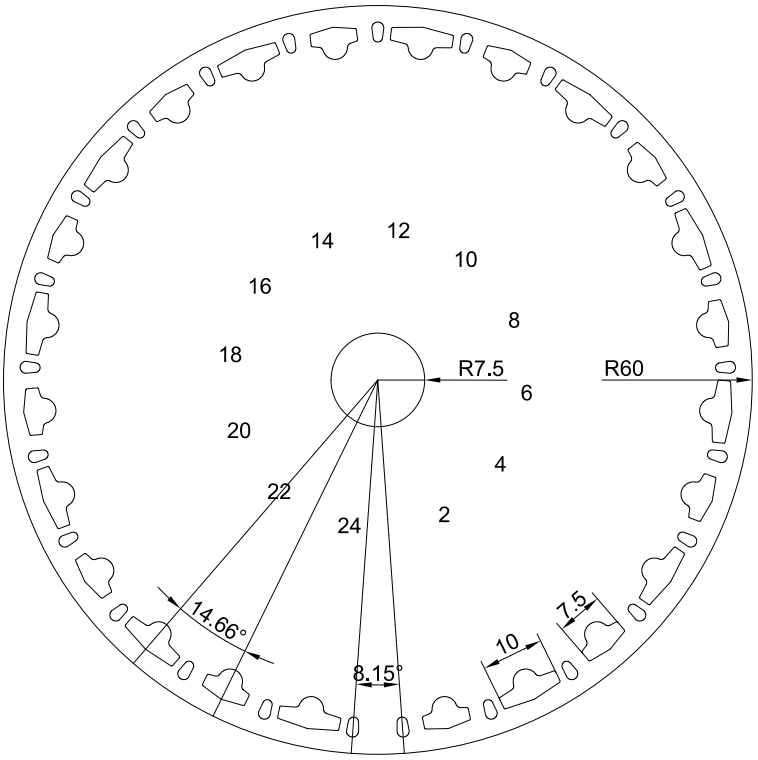

Figure 3.4: Disc with twenty four detection chambers 14.66° apart from each other. All the pair chambers are numbered in the order they will be called from now on.

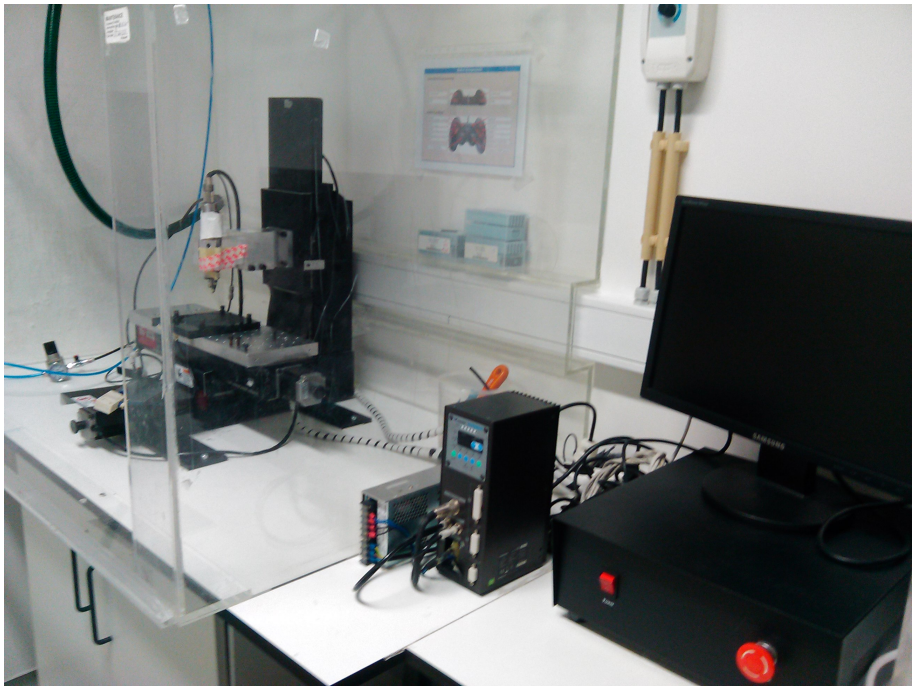

Figure 3.5: CNC room.

An alignment circumference with the same diameter as the discs' inner circumference was also cut. Then, the two disc halves were aligned so that the final part of the mixing path was placed on the top of the detection chambers, and the set was thermo-laminated once again. After the bonded disc cooled down to the room temperature, it was exposed during $1min$ to UV light and then went inside an oven for $15mins$. The final assembled disc has a blue colour. Fig.3.6 shows the assembly room, with all the equipment required for the mentioned assembly process.

Figure 3.6: Assembly room, illuminated with yellow light.

For the discs bonded with the *PC* thin layer the process was simpler. The $1.2mm$ prism discs, already with the mixing structures and all the inlets milled, were laminated with *PC* at room temperature. The discs were introduced in the laminator with chambers 2 and 24 turned to the front. Since the first lamination was not enough to obtain a perfect bonding of all the structures, a second lamination was made, this time with the disc rotated 90° from the previous lamination position.

Figure 3.7: Disc assembled with hydrophilic film.

Figure 3.8: Disc assembled with *PC*.

Fig.3.7 shows a disc assembled with hydrophilic film. Fig.3.8, on the other hand, shows a final disc assembled with *PC*.

More details are mentioned in section A.1 of Appendix A.

3.1.3 Reagents

Several reagents were tested for the Prothrombin Time test. Their main characteristics and recommended protocol are mentioned below.

Neoplastine® CI Plus* from *Stago

Neoplastine comes in two separate vials, one with $5mL$ of liquid calcium chloride, stabilisers, etc., and the other with lyophilised thromboplastin from rabbit brain. Their content has to be mixed and the result has to stabilise for about $30mins$ at room temperature, and then at 37°. Protocol indicates that for each $0.1mL$ of sample/calibrator should be used $0.2mL$ of reagent. The batch used has an *ISI* of 1.8.

In the experiments the stabilisation at 37° was not possible, and different ratios between the reagent and sample/calibrator were tested.

Thromboplastin from *Sigma Aldrich*

This reagent is a tissue thromboplastin solution from a rabbit source, meant to be used with an equal volume of $0.025M$ calcium chloride solution. Before the test the reagent has to be pre-warmed for $2mins$ at 37°, and then for each $0.1mL$ of plasma should be used $0.2mL$ of reagent.

Calcium Rabbit Brain Thromboplastin from *Diagen*

This reagent is a combination of acetone dried rabbit brain, calcium chloride, buffers and additives lyophilised that have to be reconstituted in cold distilled water. The indicated ration between plasma sample and reagent is once again 1:2.

Controls and Calibrators

Calibrators from *Stago* and *Diagen* were used. The kit from *Stago* is called *Etaloquick* and has 3 different calibrators with the values around 1.0, 2.6 and 4.0 for the *PT-INR*. These values depend on the batch used. The calibration plasma set from *Diagen* has 6 different plasmas with *PT-INR* of 0.98, 1.80, 2.83, 3.23 and 3.84. Two controls from *Stago* were also used, one normal with an expected *PT* of 11.5 - 15.0s and one abnormal, with expected *PT* of 17.5 - 25.5s.

Pipettes

The pipettes used had the following ranges: 200-1000μL, 50-200μL and 1-10μL. Pipetting errors can be a lot bigger than just the ones expected depending on the minimum value of each pipette scale. In reality, pipetting errors depend on the quality and condition of the pipette used, as well as the skill of the

person using it, the characteristics of the fluids being pipetted and also the tips used. The actual error due to pipetting is not that easy to determine. For this reason, the same set of pipettes was used in all the experiments, if possible.

Chapter 4

Results and Discussion

4.1 Preliminary tests

The first tests were made manually, in order to understand if the clot formation was visible, and whether or not the coagulation time could be determined. This turned out to be extremely difficult, because there was no immediate visible change, unless the mixture was agitated vigorously and constantly, which on the other hand made it difficult to correctly assess coagulation time. Furthermore, the final clot did not always look the same. Sometimes it was a clot ball floating in an aqueous medium, and other times it formed uniformly along the probe.

Then, taking advantage of a spectrophotometer existent in the lab, a new series of tests were made. This time the goal was to see if the reaction could be detected optically. The reagent and a normal *Stago* control were mixed and pipetted in an *ELISA* well plate, and the plate was introduced inside the device. Detection was made with light with λ = 525nm and λ = 589nm. This did not allow to see the onset of the reaction, as the beginning of detection took about 30s from the instant contact occurred. Most of the times the signal detected was a plateau.

4.2 Paired emissor-detector device

In order to see the whole reaction another system was used, represented in figure 4.1. It consists of a small opaque rectangular prism with a rectangular cavity in the middle and two small holes in opposite sides, where *LEDs* can be put. The *LED*s were connected to an electric board similar to the one inside the *spinit*®, and the commands were given through the software *Cutecom*. The results are presented in Discharge Time units (*DT*) that can be multiplied by DT_0 = 0.512μs, giving the exact time necessary for the detector *LED* to reach the threshold voltage.

Several trials were made using the reagent and the controls from *Stago*, following the preparation recommendations strictly. In the first trials, three different emission *LED*s (λ = $\{$525, 589, 433$\}nm$) from *Roithner* were tested, with different emission intensities, until variations in signal were detected. The detection *LED* used in all trials had a λ = 589 nm. Even though variations in the detected signal could

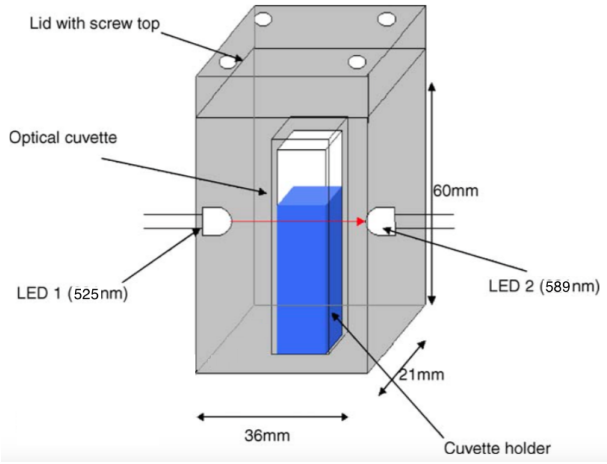

Figure 4.1: Setup used, similar to the one used in the experiment described in the article [33], source of the figure.

be detected with all three emitters, for the coagulation process, the biggest one happened for the λ = 525nm with an intensity of $\frac{40}{511} I_{max}$. This emitter was used in the same condition in the next tests. Better results might have been obtained with different emitter-detector combinations, however, as each test performed inside the cuvette requires large volumes of sample/control and reagent in order to reach the height at which the *LED*s were placed (at least a total volume of 300μL), no further trials were made in order to find the optimal conditions for each emitter.

Figure 4.2 shows an example obtained with 200 μL of a normal control from *Stago* that was added to 400μL of *Neoplastine* reagent.

The results obtained were similar in behaviour. They all show an initial *DT* state plateau that corresponds to having only the control plasma/reagent in the cuvette, then, when the reagent/plasma is introduced, we can observe an abrupt variation followed by a second *DT* state plateau with a very small negative inclination. Finally, the discharge time starts raising until a third *DT* state plateau is formed, which corresponds to the end of fibrin formation. When the first plateau is lower than the second, the control was added to the reagent already in the cuvette. If it is higher, then the reagent was added to the control.

These tests confirmed that an increase in the viscosity due to fibrin formation leads to an increase in light absorbance along the optical path, shown by the increase of the discharge times. Such behaviour is expected, as it coincides with the theory explained in chapter 2. The negative plateau observed, on the other hand, is more surprising. However, considering that there are many intermediate coagulation factors being activated before the actual fibrin formation, it means that some of the activated factors turn the medium slightly more transparent to the wavelength emitted.

A few more tests were performed to understand if the ratio between the reagent and sample altered the results. In this case the sample was a normal control (C_N). The volumes used are shown in table 4.1, as well as the coagulation times obtained and the nornalised ΔDT_{Coag}, both defined in section B.1.1.

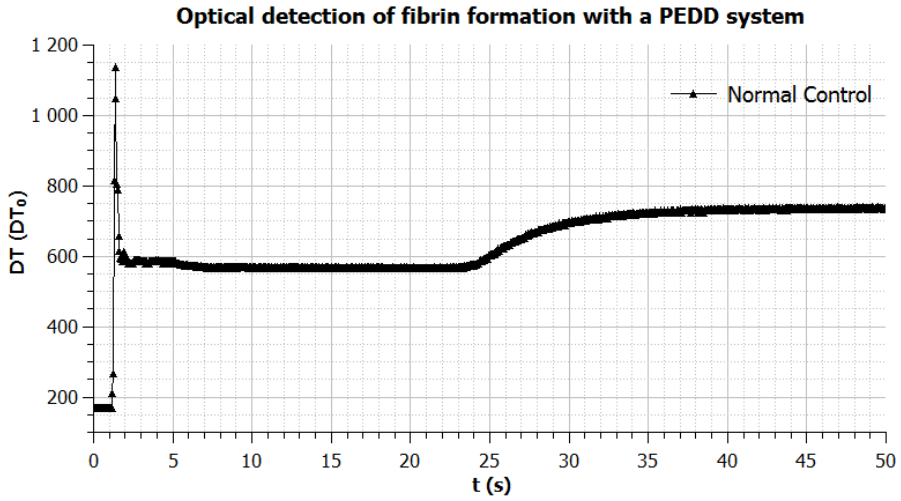

Figure 4.2: Optical detection of fibrin formation of a normal control plasma from *Stago* with *Neoplastine*.

Ratio S:R	1:1	1:2	1:3	1:4
C_N (μl)	150	300	450	600
Reag (μl)	150	150	150	150
$\Delta DT_{Coag_{norm}}(\%)$	19.58	15.73	15.18	8.69
t_{Coag} (s)	16.16	17.63	19.43	24.19

Table 4.1: Coagulation times defined in section B.1.1 for different Sample:Reagent proportions (ratio S:R). The volumes used to understand the impact of the alteration of the recommend protocol of the reagent are also shown.

The results show that using more reagent for the same volume of control plasma increases the coagulation time. It also alters the signal variation observed, which gets smaller for smaller S:R ratios. At the time this test was made, having a bigger signal variation and also being able to use lower reagent volumes seemed a better option. Therefore, the S:R ratio used in further tests until otherwise mentioned is 1:1.

Finally, the possibility of diluting the reagent was also explored. The reagent was diluted in distilled water in the proportions $V_{Reagent} : V_{Reagent+H_2O}$. The smaller the ratio, the bigger is the dilution. The normalized ΔDT_{Coag} and coagulation times for each dilution tested are shown in table 4.2.

Dilution	1:1	1:1	1:2	1:2	1:5	1:5	1:10	1:10
$\Delta DT_{Coag_{norm}}(\%)$	16.26	21.50	16.30	18.48	11.31	8.09	7.29	6.61
t_{Coag} (s)	24.72	23.37	25.82	27.92	33.41	30.38	41.23	38.61

Table 4.2: Coagulation times defined in section B.1.2 for different dilutions of the reagent. The Sample/Reagent proportion used is 1:1.

Table 4.2 shows that coagulation times increased for bigger dilutions. The nornalized ΔDT_{Coag} did not vary significantly between the tests using the reagent directly and the ones using the 1:2 dilution. For bigger dilutions the coagulation signal variation decreases. As mentioned before, at this stage using

less reagent seemed a better option. Therefore, the 1:2 dilution was used in further tests until otherwise mentioned.

4.3 Tests with *spinit*®

Meanwhile, the company acquired a new double-beam spectrophotometer, Hitachi U-2900, that can read transmittance with wavelengths ranging from 190nm to 1100nm. This spectrophotometer came with a set of cells for very small volumes, all of them with an optical path of 1cm. A 50μL cell was chosen to study the variation of the transmittance during fibrin formation, for different emitting wavelengths. All the reactions consisted on mixing 40μL of diluted reagent with 40μL of a normal control plasma, and placing the mixture inside the detection cell. The whole process took approximately 15 $\pm$ 2s. For wavelengths above 500 nm replicates were made.

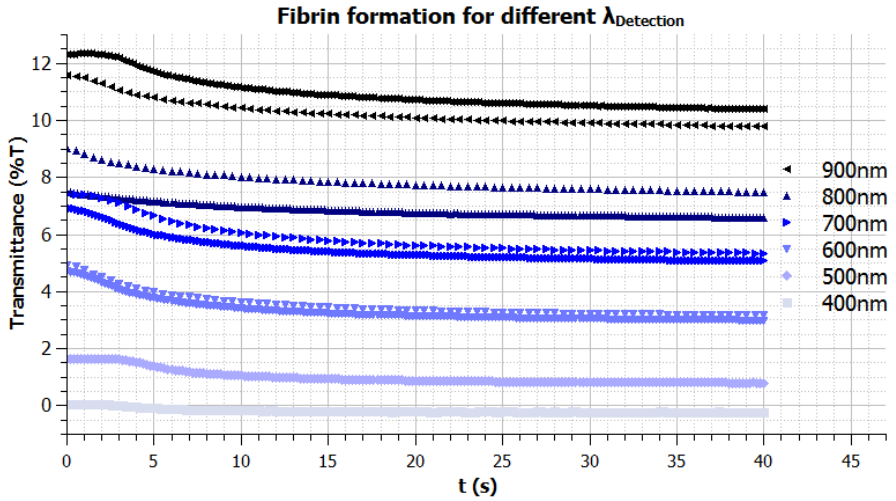

Figure 4.3: Transmittance variation during coagulation for different emitting wavelengths using the double-beam spectrophotometer.

Unlike the results obtained with the *LED*s inside the black box, in this case the reactions are not seen from the beginning, as the reagent and control had to be mixed outside the detection cell. The results presented in figure 4.3 show that each test starts at a different phase of the coagulation process. The beginning of the coagulation process occurs very fast, and a $\pm$ 2s error in the first measurement instant can explain the different phases captured in the initial detection instant, and also the fact that some replicates look so different. For the wavelengths above 500nm the transmittance variation during fibrin formation was practically the same, no matter the wavelength, despite the fact that for higher wavelengths the transmittance values are higher.

The main goal of this test was to understand if the *PT* assay could be performed using an emitter *LED* with λ = 605nm, since this is a wavelength that has already been studied and characterised when

used inside the *spinit*®. Fortunately, the results shown in figure 4.3 prove that this specific wavelength allows to observe a significative signal variation during fibrin formation. Therefore, the next step was to perform tests using the *spinit*®.

The coagulation times obtained in the previous tests, performed with a normal control, were sometimes lower than $20s$, depending on the protocol used. Such short times demand an almost instantaneous efficient mixing of the reagent and sample, a very fast delivery to the detection chamber, and also a fast way of finding the chamber where the reaction is taking place. These three aspects were the main concern at this point, and the basis for further testing.

4.3.1 Mixing Structures

Mixing layout 1

A first layout that consisted of basic mixing structures was made, shown in figure 4.4. It was meant to test the quality of the mixture of equal volumes of control plasma and reagent. The construction used was the first one mentioned. Structures 5 and 6 were thought of in order to understand the influence of the intervening fluids' viscosities in the mixing process. The main goal was to see whether the reagent was more or less viscous than the plasma, and then, try to add the denser fluid on top of the other, to see if the deposition was, on its own, enough to obtain a homogeneous mixture. Structures 1 and 2 were meant to understand if the contact between reagent and plasma inside a straight, narrow delivery channel lead to a good enough mixture. Finally, structures 3 and 4 were based on the structure proposed by Ju-Nan Kuo and Bo-Shiun Li in 2014. All structures are $200\mu m$ deep and have a $0.508mm$ width.

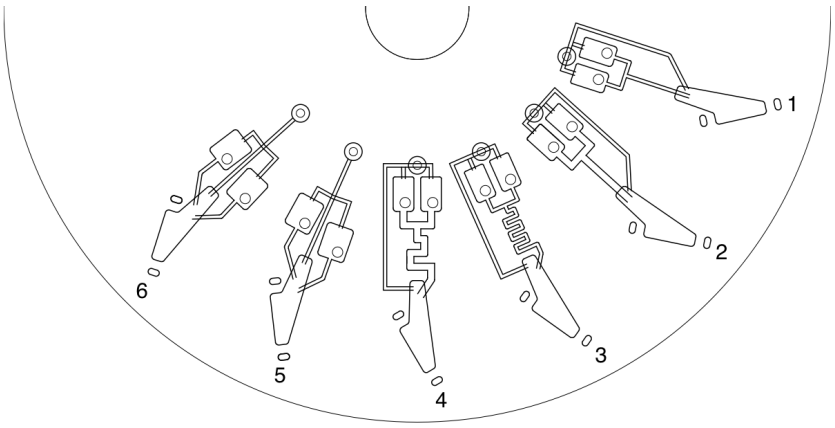

Figure 4.4: First microfluidic disc layout. The structures were milled with a milling cuter with a $0.508mm$ diameter.

Before testing this layout inside the *spinit*®, a disc was tested in a simpler device that consists of an open disc drive and a camera that relies on a tracking system to capture sequential images of the same disc position as time passes. All the structures were tested with coloured water and reagent, as coloured

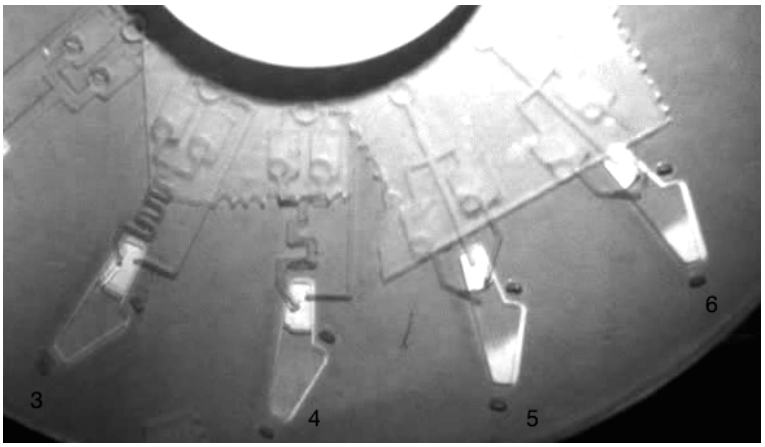

Figure 4.5: Results for the first microfluidic disc layout using equal volumes of coloured water and Neoplastine reagent, after a 5s rotation at 1000rpm.

water has a similar density to that of plasma, approximately 1025Kg/m^3, and the mixing process was seen in real-time.

Figure 4.5 shows the results obtained in chambers 3 to 6, after rotating the disc for 5s at 1000rpm. Structures 5 and 6 resulted in very heterogeneous final results, with the reagent occupying the bottom of the chamber. Structures 1 and 2 also resulted in a very heterogeneous final result that is not shown, similar to the one obtained with structures 5 and 6. Structures 3 and 4 resulted in more homogeneous mixtures, from which the first one is the best. This structure was chosen to perform the study of the different reagents in-house inside the *spinit*®.

Reagents comparison

Thromboplastins from three different brands was tested: *Stago*, *Sigma* and *Diagen*. It is relevant to say that all three reagents are meant for mechanical detection of clot formation. After a basic preparation of each reagent, the one from Sigma was excluded as an option, as it turned out to be very heterogeneous, with visible particles in suspension. A closeup is shown in figure 4.6.

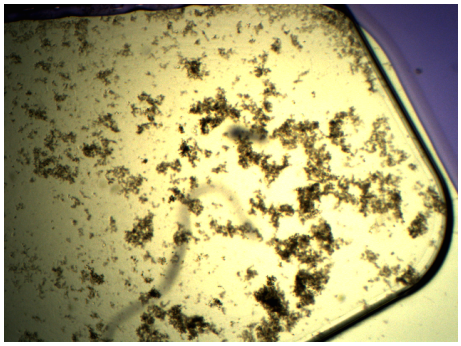

Figure 4.6: Closeup of the Sigma reagent inside a detection chamber.

Both reagents from *Stago* and *Diagen* were tested with the calibrators available from each brand. The reagent was introduced inside the left chambers and the calibrator plasmas inside the right ones. The holes were then sealed with duct tape, and the disc was introduced inside the drive. The results are shown in section B. The ones obtained with the reagent from *Diagen* did not show a perceptible pattern. The reagent from *Stago*, on the other hand, allowed to obtain curves that showed a similar behaviour for all different calibrators. The fact that this was the first reagent to arrive and to be used in the previous tests turned out to be very fortuitous. All the tests were performed at room temperature, 25° at the time, since the*spinit*® used was open.

Despite the fact that the third structure of the first layout was the one that allowed to obtain a better mixture, this structure was still not ideal, as the mixture obtained in the detection chamber after each test was not homogeneous to the naked eye. The lack of homogeny of the final mixture might explain the imprecision values of the coagulation times obtained when mixing 4.5μL of the dilution of *Stago* reagent in purified water (1:2) with 4.5μL of plasma.

The coefficient of variation (*CV*) was determined for each calibrator value, using the formula 4.1.

$$CV = \frac{\sqrt{\frac{\sum_{i=1}^{N}(x_i - \bar{x})^2}{N-1}}}{\bar{x}} \tag{4.1}$$

N is the number of duplicates considered, and $\bar{x}$ is the average of all the results considered.

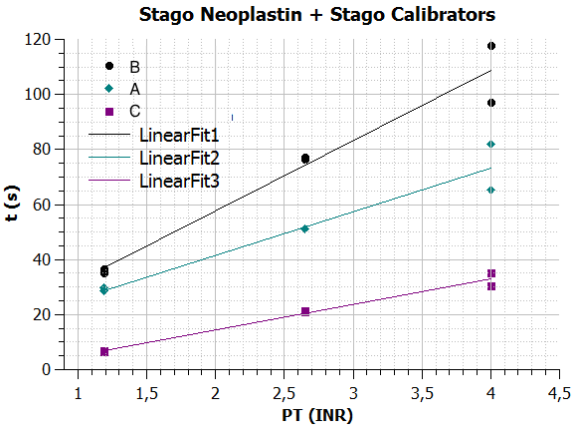

Figure 4.7: Calibration curves for structure 3 of the 1st mixing layout.

Time Reference	INR	1.19	2.65	4.00
A	CV (%)	2.61	0.34	16.02
B	CV (%)	2.34	0.46	13.60
C	CV (%)	1.19	0.71	8.36

Table 4.3: Coefficient of variation for different time references (*A*, *B* and *C*), for all three *Stago* calibrators. The results were obtained with structure 3 from the 1st mixing layout.

Two tests were run for each calibrator, and the data was analysed in different ways, in order to understand how the coagulation times could be extracted from a curve partially similar to that shown in figure 4.2. A detailed explanation of the analysis made to the raw data is presented in section C.1. The calibration curves obtained for all three different coagulation time references are shown in figure 4.7. Table 4.3 has the *CVs* obtained for each calibrator, for all three time references.

Mixing layout 2

In order to obtain a more efficient mixing, with original structures, a new layout was made, shown in figure 4.8. Once again the construction scheme of the discs was the same as the one used for the previous layout. This layout consisted of slightly more complex structures, that make the reagent and sample split and collide several times before reaching the detection chamber. All the structures are 200μm deep and also have a 0.508mm width. Structures 6 and 4 even have several channels coming out of the inlet chambers, which are then linked to the main structure at different radius, in order to allow the reagent and sample to alternate in the main channel.

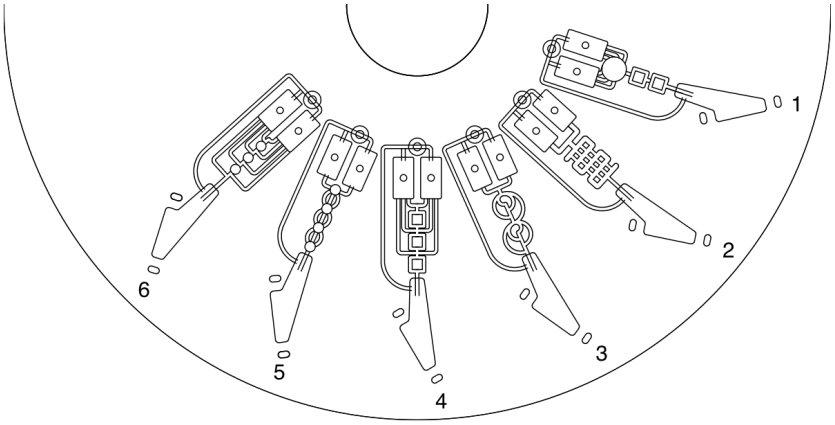

Figure 4.8: Second microfluidic disc layout. The structures were milled with a milling cuter with a 0.508mm diameter. Tests were made at 25°.

Two different coagulation time references, *A* and *B*, were determined for each structure. The results for each time reference are shown in figures 4.9 to 4.14.

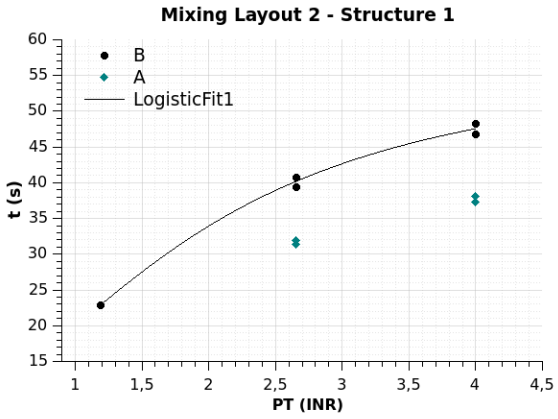

Figure 4.9: Results for structure 1 of the 2nd mixing layout.

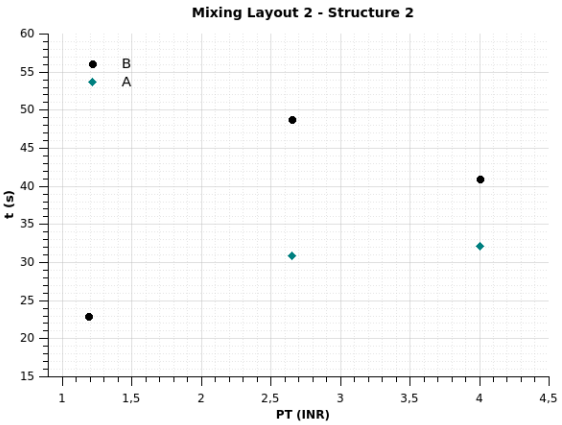

Figure 4.10: Results for structure 2 of the 2nd mixing layout.

Even though three repetitions were made for each calibrator in each structure, several results were lost because the chamber was not detected in time. This required a revision of the centrifugation protocol used and also the settings of the *PEDD* setup, in order to optimise the whole system for this type of

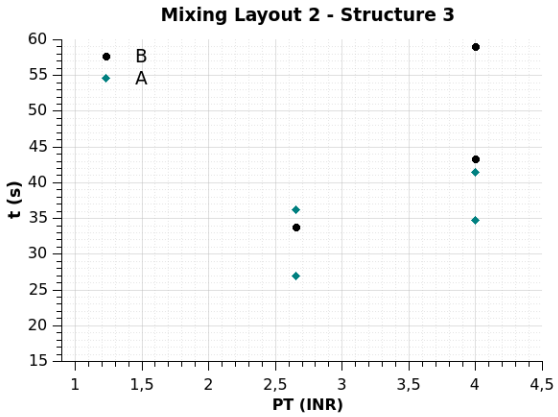

Figure 4.11: Results for structure 3 of the 2nd mixing layout.

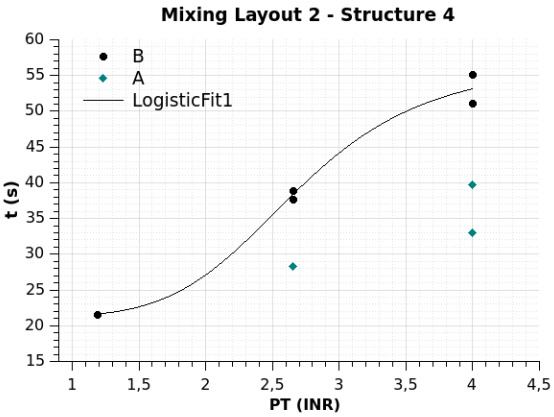

Figure 4.12: Results for structure 4 of the 2nd mixing layout.

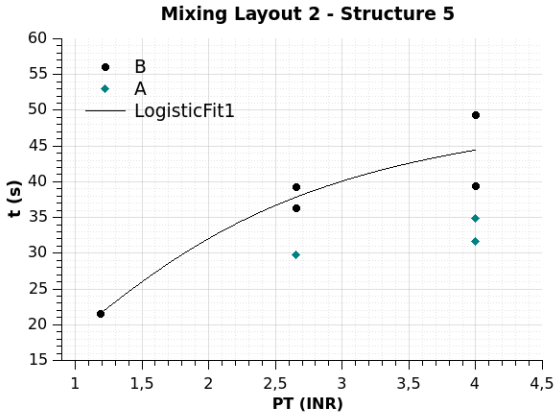

Figure 4.13: Results for structure 5 of the 2nd mixing layout.

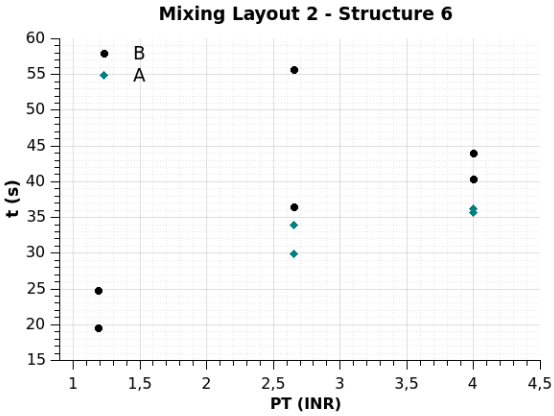

Figure 4.14: Results for structure 6 of the 2nd mixing layout.

reaction. Also, no further tests were made because the number of discs available was limited. Each disc took about 15$mins$ to make, and the equipment required was not always available.

In this case, the determination of the *CV*s in order to compare the structures and the best time reference used did not make sense. In fact, for most of the structures there are no replicates for time reference *A*, which makes it difficult to compare the results with the ones obtained with time reference *B*. Nevertheless, it is evident that they vary a lot by the results obtained for the 5th structure with the 2.65INR calibrator, for instance, shown in figure 4.14.

Some conclusions could still be made. First of all, from the few results for the second structure, it seems that the mixture is not properly done, since the result for the calibrator with an *INR* of 2.65 is very similar to the result obtained with the 4.00 calibrator, if time reference *A* is considered, and is higher than it, if time reference *B* is considered. A similar logic can be applied to the results obtained for structure 3, which also reflect a bad mixing. In fact, these two structures were the ones that originated the most heterogeneous mixtures in the detection chamber, which corroborates the results. Structures 1 and 4, on the other hand, were the ones that allowed to obtain coagulation times with the expected pattern, meaning that for the calibrators with higher *INR* values, the coagulation times obtained were

also higher, for both time references considered. This similarity in behaviour, for both time references, is very important. Structure 1 was still the best one, although it is interesting to notice that both structures are square shaped. The results for structures 5 and 6 also show an expected pattern, although the imprecision between replicates is clearly bigger than the one obtained for structures 1 and 4.

Mixing layout 3

The previous results were not exceptionally conclusive, which led to the necessity to further study the serpentine structure. A third mixing layout was made, to understand how much the mixing quality changes when using serpentine structures with different depths, widths, number of turns, etc. The construction scheme used was similar to that used for the previous layouts. The layout of the disc is shown in figure 4.15. Structure number 6 was chosen as the reference structure. It has a 0.508μm wide channel that is 200μm deep. Structure 2 is similar to structure 6 except in depth, which is 300μm. Structures 5, 4 and 3 are all 200μm deep and also have a channel with a 0.508μm width. The variables that change when compared to the reference structure are the number of turns, width of the turns and shape of the turns, respectively. Finally, structure 1 has a bigger width than structure 6.

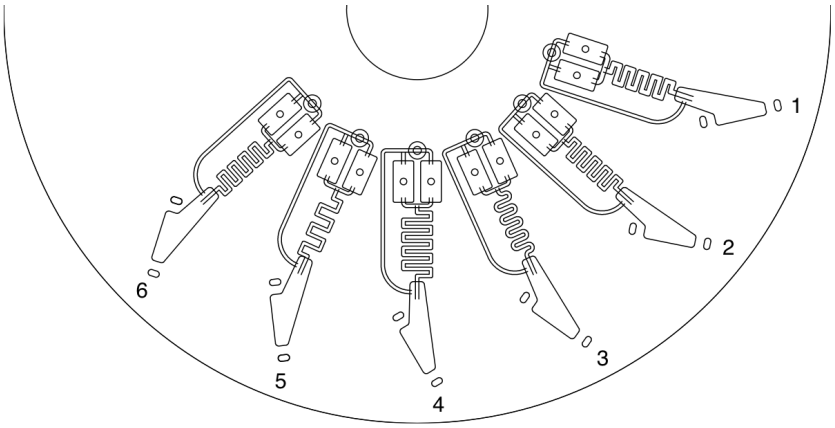

Figure 4.15: Third microfluidic mixing disc layout. The structures were milled with a milling cuter with a 0.508mm diameter. Tests were made at 24°.

The results obtained for each structure are shown in figures 4.16 to 4.21.

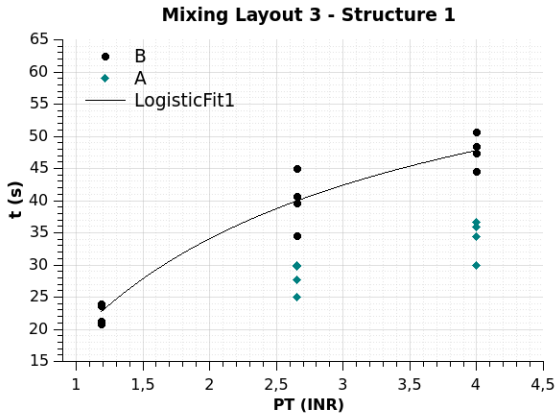

Figure 4.16: Results for structure 1 of the 3rd mixing layout.

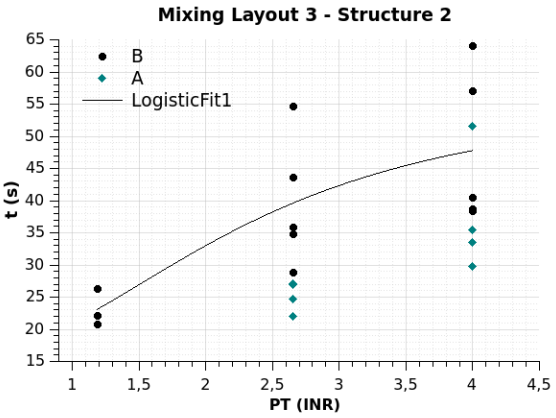

Figure 4.17: Results for structure 2 of the 3rd mixing layout.

Despite the changes made to the protocol and system settings, the minimum time detected was often

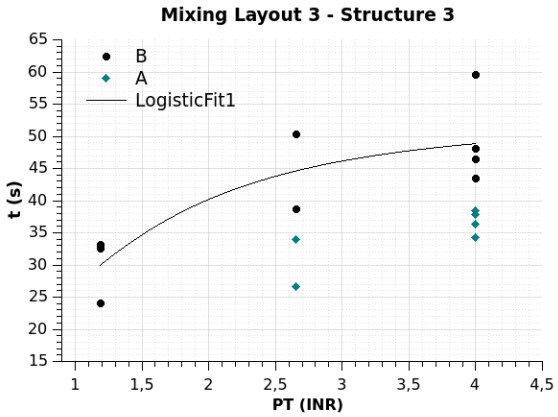

Figure 4.18: Results for structure 3 of the 3rd mixing layout.

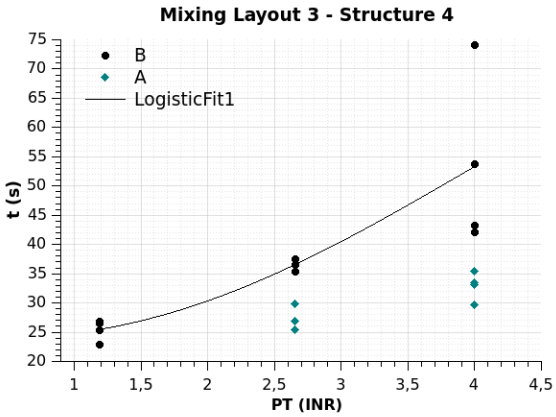

Figure 4.19: Results for structure 4 of the 3rd mixing layout.

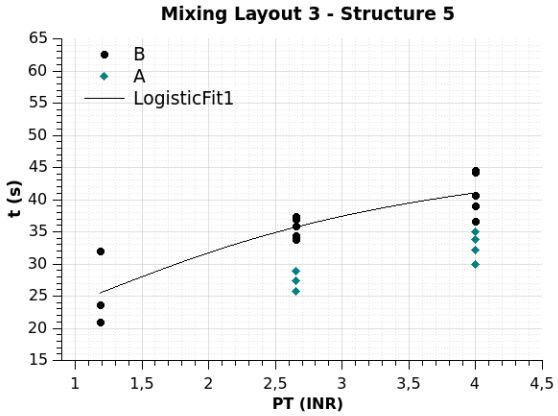

Figure 4.20: Results for structure 5 of the 3rd mixing layout.

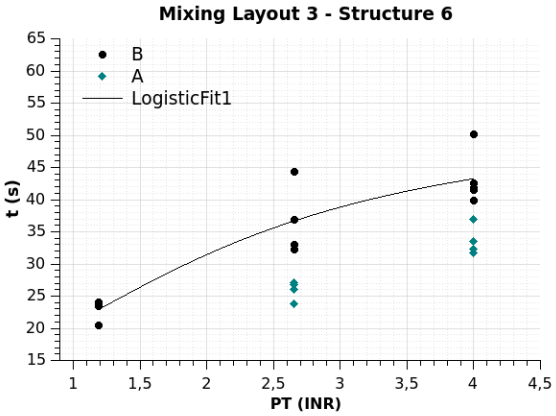

Figure 4.21: Results for structure 6 of the 3rd mixing layout.

slightly higher than 20s, which did not allow to obtain the coagulation times for the lower calibrator, with an $INR = 1.19$, for time reference *A*.

The coagulation times obtained in this section are slightly smaller than the ones obtained with the first layout. This variation can be explained by the difference in the *ISI* of the reagent vial used, which varies from batch to batch.

This time, 5 replicates were made for each calibrator, for each structure. Once again, some results could not be obtained because the chamber was not correctly identified in time, (5 in 90 times), which required further changes in the detection protocol. Also, in other cases, the signal obtained did not show the expected behaviour, so the reference instants could not be determined (8 in 90 times). This might have to do with the reagent dilution not being completely homogeneous.

All the points per reference value were considered in the determination of the *CVs*, despite the fact that the number of replicates is not the same for every calibrator, for each structure. This means that the results can not be strictly compared to each other, allowing to make only qualitative comparisons.

The data presented in tables 4.4 and 4.5 shows that when the *CVs* of a specific structure and regarding one of the time references is more or less similar between calibrators, then the correspondent

INR	Structure	1	2	3	4	5	6
1.19	CV (%)	-	-	-	-	-	-
2.65	CV (%)	8.34	9.23	16.94	8.29	5.76	5.82
4.00	CV (%)	8.75	25.65	4.96	7.28	7.04	7.07

Table 4.4: Coefficient of variation of the time reference *A*, for all three *Stago* calibrators, for each structure of the 3rd layout.

INR	Structure	1	2	3	4	5	6
1.19	CV (%)	7.51	12.26	-	6.48	38.73	6.93
2.65	CV (%)	10.75	25.05	18.36	2.92	4.33	15.07
4.00	CV (%)	5.34	25.09	12.76	27.85	8.24	9.23

Table 4.5: Coefficient of variation of the time reference *B*, for all three *Stago* calibrators, for each structure of the 3rd layout.

CVs for the other time reference varies significantly. There is no apparent reason, and this could be a coincidence only. Also, for all the structures, except for structure 2, the *CVs* are more consistent for the time reference *A*. This time reference could be considered the best way of determining the *PT*. However, it is not useful if the times for small *INR* values can not be detected, which so far is often the case. Structure 2 gave the worst results, based on the high *CVs* for all the calibrators, for both time references. Structure 3 also seems to originate bad results, despite the fact that for the $INR = 4.00$ calibrator the four replicates originated a *CV* of only 4.96%, for the time reference *A*.

The data available is not enough to evaluate which structure is the best. Nevertheless, it reveals that the reactions were influenced by some kind of interferent, which could possibly be the hydrophilic film.

Mixing Layout 4

Finally, one last layout was tested, which included modifications not only in the mixing structures, but also in the detection chambers. In this case the mixing structures were milled in 1.2mm discs that already have the detection chambers and prisms, and a thin *PC* layer was put on top, to seal the disc. The layout is shown in figure 4.22. Structure number 12 was chosen as the reference structure, since its dimensions are similar to the ones of the reference structure of the previous mixing layout. It has a 0.508μm wide channel that is 200μm deep. However, the position of the structure is different, since it is further away from the disc centre. All structures have 0.508μm channels that are 200μm deep. Structures 8 to 12 and 18 were included in order to have a link between this completely new layout and the third mixing layout described before, which did not provide conclusive results. Structures 4, 14, 16 and 20 were thought of in order to make the fluid go through a channel that gets narrower and larger several times while the fluid is being pulled outwards the centre of rotation. In these structures the narrower parts are 0.508μm wide, whilst the larger ones are three times larger. Structures 2, 6 and 24 lead to fluid separation and collision in three different places.

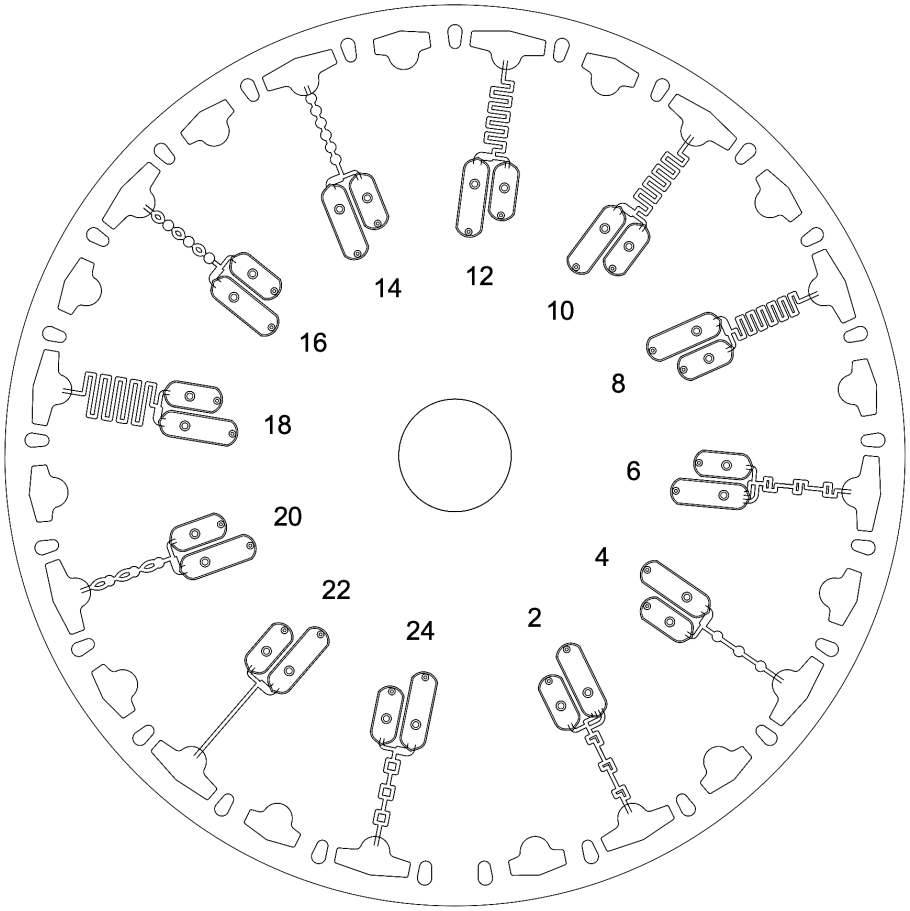

Figure 4.22: Fourth microfluidic mixing disc layout. All structures were milled with a milling cuter with a $0.508mm$ diameter. Tests were made at the fixed temperature 35°.

In this test the proportion of reagent and sample used was altered. $2.5\mu L$ of sample were used with

$5\mu L$ of reagent. This change was made in order to use less plasma per test. In the beginning of this study one of the main concerns was trying to use the smallest volume of reagent possible. However, since this test is being developed so that it can eventually be incorporated in an existing assay panel, the the main concern is now using the smallest volume of sample possible, whilst still being able to fill the whole detection chamber.

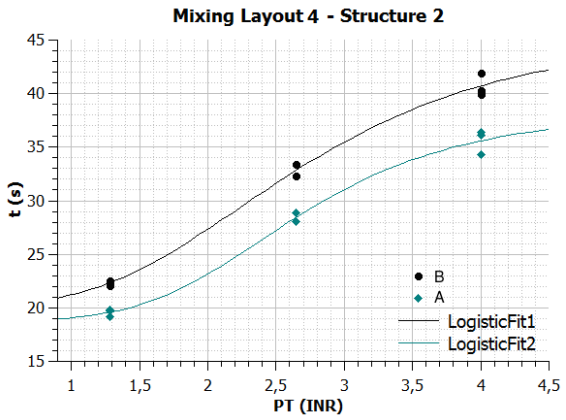

Figure 4.23: Calibration curves for structure 2 of the 4th mixing layout.

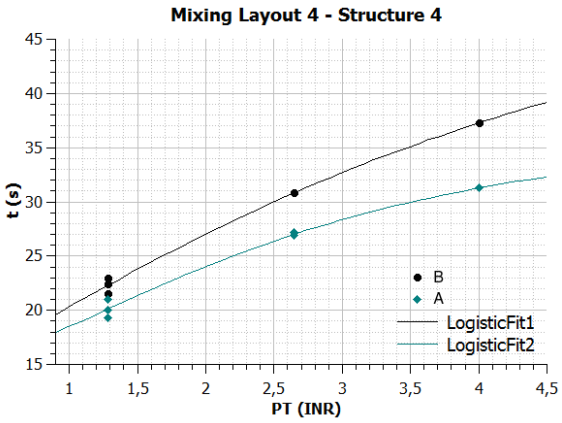

Figure 4.24: Calibration curves for structure 4 of the 4th mixing layout.

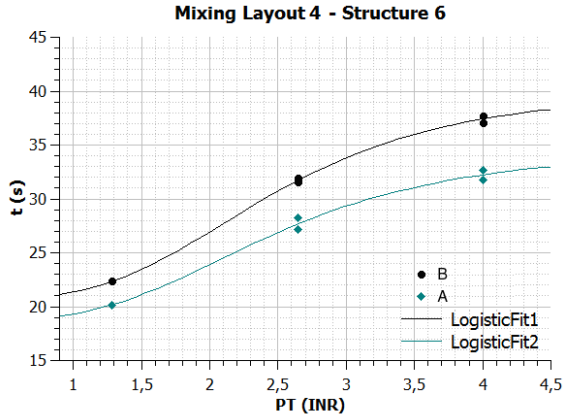

Figure 4.25: Calibration curves for structure 6 of the 4th mixing layout.

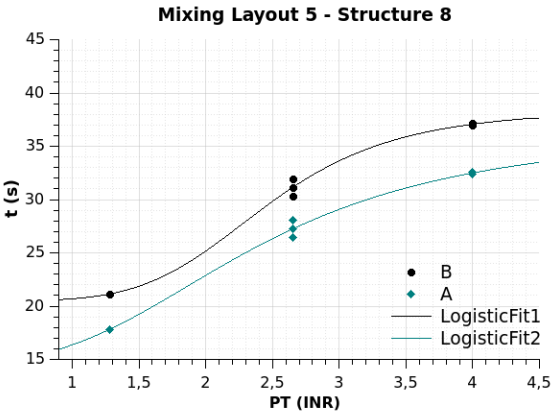

Figure 4.26: Calibration curves for structure 8 of the 4th mixing layout.

Each calibrator was tested in triplicate, for each structure. In some tests the chamber was not detected in time to observe any of the two time references. These results were discarded. Also, unlike what happened in the third mixing structure study, in this case all the signals detected behaved in an expected way.

The *CVs* shown in tables 4.6 and 4.7 were determined with two points. They are the worst case scenario, since they were determined with the two points that are further from each other, for each *INR* value, for each structure. Also, in some cases the reference time was assumed to be the first instant of detection, when the time reference was not detected in time, but still seemed to have occurred almost immediately before the first moment of detection. This contributes to having calibration curves that may result in a loss of range near the lowest INR values.

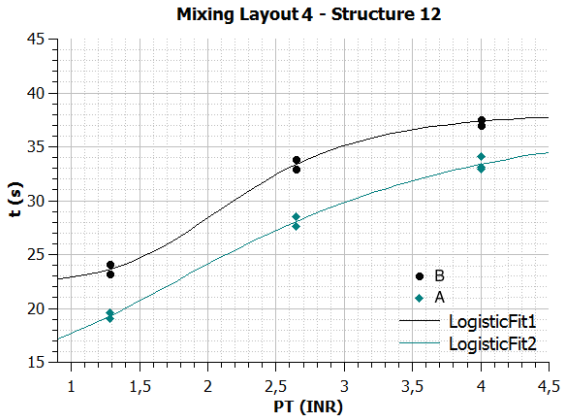

Figure 4.27: Calibration curves for structure 12 of the 4th mixing layout.

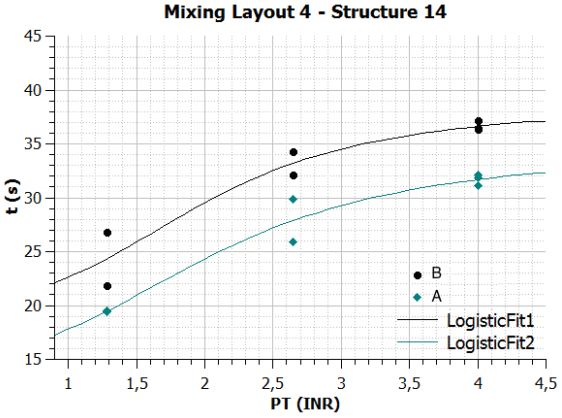

Figure 4.28: Calibration curves for structure 14 of the 4th mixing layout.

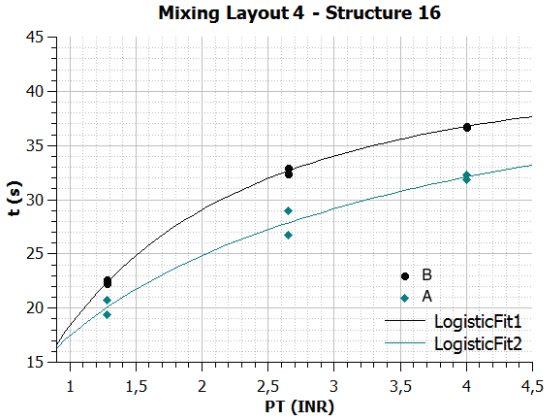

Figure 4.29: Calibration curves for structure 16 of the 4th mixing layout.

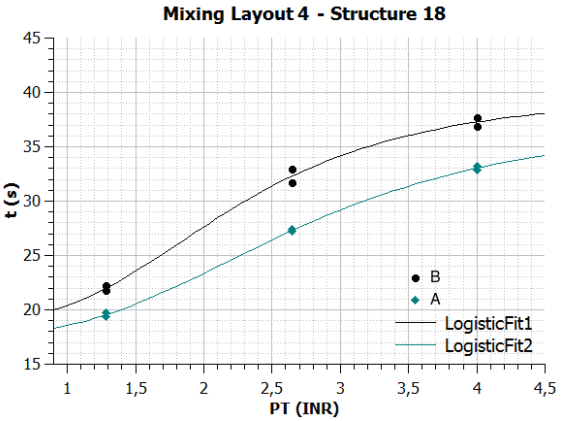

Figure 4.30: Calibration curves for structure 18 of the 4th mixing layout.

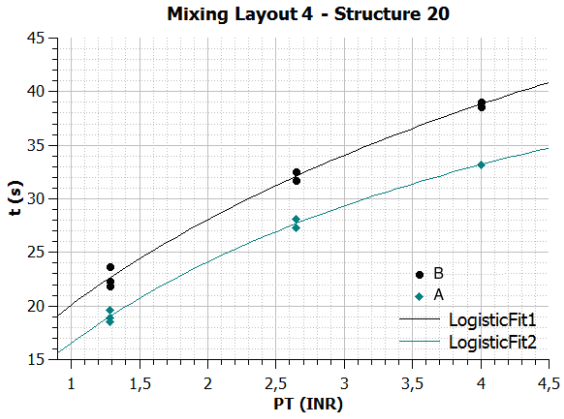

Figure 4.31: Calibration curves for structure 20 of the 4th mixing layout.

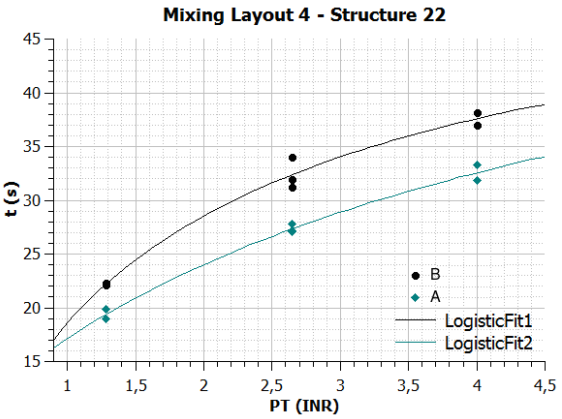

Figure 4.32: Calibration curves for structure 22 of the 4th mixing layout.

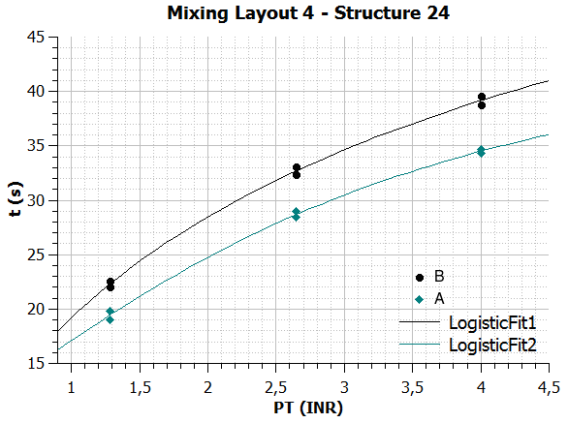

Figure 4.33: Calibration curves for structure 24 of the 4th mixing layout.

INR	Structure	2	4	6	8	12	14	16	18	20	22	24
1.28	CV (%)	16.41	15.94	-	-	4.59	0.14	8.75	5.45	7.10	6.47	5.56
2.65	CV (%)	2.56	1.73	5.32	7.46	4.42	24.00	14.68	0.90	4.14	4.19	2.38
4.00	CV (%)	12.97	-	8.21	1.76	7.71	10.93	3.43	2.18	-	8.23	2.15

Table 4.6: Coefficient of variation of the time reference *A*, for all three *Stago* calibrators, for each structure of the 4th layout.

INR	Structure	2	4	6	8	12	14	16	18	20	22	24
1.28	CV (%)	4.92	11.71	-	-	14.65	46.73	1.63	4.04	11.30	0.76	2.66
2.65	CV (%)	3.67	0.17	1.25	5.09	3.64	13.64	3.52	5.34	3.45	15.07	3.24
4.00	CV (%)	9.60	-	4.69	1.12	8.95	11.59	0.95	7.20	1.78	6.93	3.56

Table 4.7: Coefficient of variation of the time reference *B*, for all three *Stago* calibrators, for each structure of the 4th layout.

Once again, the results obtained with each structure from every mixing layout are not enough to make a statistical study of the efficiency of each structure. This could be done if the experiment was repeated several times, so that the inter- and intra-assay imprecision could be determined and studied. It is still possible to understand which structures create a better mixing, based on the data collected, keeping in mind that future repetitions of the experiment should be done in order to confirm the results.

Using this new layout, almost all the *CVs* determined were significantly lower than the ones obtained using the third mixing layout. Structure 14 was the one that clearly originated the worst mixing, with *CVs* for almost all the calibrators, for both time references higher than 10%. The very low *CV* for the 1.19 *INR* calibrator using time reference *A*can be explained by the fact that both times used in its determination were considered the first detection instant, which was very similar. One might expect that a simple straight channel such as structure 22 would originate the worst mixing. However, structure 22 turned out to originate more precise replicates than structure 14, which incorporates width variations of the channel. There are two possible reasons. First of all, structure 14 is globally larger than structure 22,

which eventually leads to a decrease in the contact area between the two fluids. Secondly, in a straight narrower channel, the air passing from the detection chamber to the air holes can contribute to mixing.

Globally, no time reference can be considered better than the other, based exclusively on the results shown. For structures 18, for instance, time reference *A* originated lower *CVs* than time reference *B*. For structure 16 the opposite is true.

The mixing structure which consistently gave low *CVs* for all three calibrators, for both time references, is structure 24. This consistency is a good indicator of the structure mixing potential. Similarly to the serpentine structures, structure 24 is also very simple, which is advantageous in a manufacturing point of view. However, several other structures could be considered just as good. Structures 18 and 20, for instance, also originated precise duplicates, and the fits obtained for both time references would have had a more similar shape if time reference A had not been extrapolated form first detection instants. Also, different calibration curves could have improved the *CVs* for some of he structures.

It is interesting to observe that the coagulation times do not vary much between some of the structures, for the same calibrator and time reference, which is a good indicator that the system used originates reproducible results.

The acceptability of the results depends on the analytical error allowable, which is 15% total error for the *PT*. However, the determination of the total error requires that real samples are tested, which is why it was not determined in this study.

Chapter 5

Conclusions

As was mentioned before, the development of mixing structures that allow rapid and efficient mixing is essential in microfluidics. In the specific case of coagulation assays, the time required is especially important, since the coagulation process can occur within a few seconds only.

The results shown in the previous section confirm that a structure as simple as a serpentine can allow to obtain more homogeneous mixtures than more complex structures. If two similar volumes of fluids with relatively similar densities are pushed towards the outer radius almost simultaneously, through a path that offers some kind of resistance, then the fluids will be better mixed than if they were simply directly introduced in the detection chamber through a large channel. The resistance can be provoked by forcing the fluid movement to change direction, by narrowing the channels in which the fluids travel, or by inducing fluid separation and collision.

The *CVs* obtained for some of the structures were very low, within the specified analytical performance criteria. However, more replicates in different days are needed to assure the system performance. For the Prothrombin Time, the total error allowed is 15%. However, since no real samples were tested, no total errors were determined.

5.1 Future Work

The results obtained in this study are encouraging, especially taking into account that this particular assay is usually performed with mechanical or electrochemical detection methods. To our knowledge, there is only one single point of care device that uses optical detection to determine the *PT*, and it requires larger sample volumes and a more complex sample preparation. Also, its detection method relies on determining the difference in the absorbance of the sample before and after the coagulation occurs, which is an approach significantly different from the one studied. The *PT* can be easily misdetermined in samples that have a high concentration of lipids and bilirubin, or have suffered hemolysis. Mechanical methods are not so sensitive to these interferents, but optical methods are prone to inaccuracies for such samples. The proposed optical method, however, can overcome this issue, since the *PT* determination is not based on specific optical variations. Instead, it relies on the behaviour of such variations

throughout time, which is a completely new approach.

The immediate next step will be performing this assay with real plasma samples and then using capillary blood, provided in real time. The next big step will be the implementation of an optimised version of this system into a disc with all the microfluidic necessary to separate whole blood into blood cells and plasma, reconstitute dried reagents, and also meter the necessary volumes. Such microfluidic structures have already been developed in *biosurfit*. Small adjustments should be enough to obtain a first draft disc that allows to obtain coagulation times from a single drop of capillary blood. An automatic preparation of the sample should contribute significantly to lower the imprecision of the system. However, drying and reconstituting reagents could be an additional error source.

A further study is needed to understand the impact of the malfunction of each coagulation factor of the extrinsic path in the overall coagulation signal obtained. This study could also help understand if t is possible to detect malfunctioning factors doing a single *PT* test using the method described in this study, instead of individual tests with different reagents, for each factor.

The results of this study are now being further developed within the scope of a new project in *biosurfit*.

Bibliography

[1] J.-N. Kuo and B.-S. Li. Lab-on-cd microfluidic platform for rapid separation and mixing of plasma from whole blood. *Biomedical microdevices*, 16(4):549–558, 2014.

[2] C. T. Schembri, V. Ostoich, P. Lingane, T. Burd, and S. Buhl. Portable simultaneous multiple analyte whole-blood analyzer for point-of-care testing. *Clinical chemistry*, 38(9):1665–1670, 1992.

[3] C. D. Chin, S. Y. Chin, T. Laksanasopin, and S. K. Sia. Low-cost microdevices for point-of-care testing. In *Point-of-Care Diagnostics on a Chip*, pages 3–21. Springer, 2013.

[4] C. D. Chin, V. Linder, and S. K. Sia. Lab-on-a-chip devices for global health: Past studies and future opportunities. *Lab on a Chip*, 7(1):41–57, 2007.

[5] M. Madou, J. Zoval, G. Jia, H. Kido, J. Kim, and N. Kim. Lab on a cd. *Annu. Rev. Biomed. Eng.*, 8: 601–628, 2006.

[6] C. Mathers, D. M. Fat, and J. T. Boerma. *The global burden of disease: 2004 update*. World Health Organization, 2008.

[7] M. Faivre, P. Peltié, A. Planat-Chrétien, M.-L. Cosnier, M. Cubizolles, C. Nougier, C. Négrier, and P. Pouteau. Coagulation dynamics of a blood sample by multiple scattering analysis. *Journal of biomedical optics*, 16(5):057001–057001, 2011.

[8] L. Sherwood. *Human Physiology - From Cells to Systems*, volume 1. Brooks/Cole, 7 edition, 2010.

[9] L. Enriquez and L. Shore-Lesserson. Point-of-care coagulation testing and transfusion algorithms. *British journal of anaesthesia*, 103(suppl 1):14–22, 2009.

[10] G. D. Boon. An overview of hemostasis. *Toxicologic pathology*, 21(2):170–179, 1993.

[11] M. Shuman and C. S. Greenberg. Platelet regulation. *Biochemistry of Platelets*, pages 319–346, 1986.

[12] J. D. URL `http://en.wikipedia.org/wiki/Coagulation#mediaviewer/File:Coagulation_full.svg`.

[13] R. G. Macfarlane. An enzyme cascade in the blood clotting mechanism, and its function as a biological amplifier. *Nature*, (202):498 – 499, May 1964.

[14] M. Hoffman and D. M. Monroe. Coagulation 2006: a modern view of hemostasis. *Hematology/oncology clinics of North America*, 21(1):1–11, 2007.

[15] J. Vermylen, M. Verstraete, and V. Fuster. Role of platelet activation and fibrin formation in thrombogenesis. *Journal of the American College of Cardiology*, 8(6s2):2B–9B, 1986.

[16] C. Hillyer, K. L. Hillyer, F. Strobl, L. Jefferies, and L. Silberstein. *Handbook of transfusion medicine*, volume 1. Academic Press, 1 edition, 2001.

[17] J. Horsti, H. Uppa, and J. A. Vilpo. Poor agreement among prothrombin time international normalized ratio methods: comparison of seven commercial reagents. *Clinical chemistry*, 51(3):553–560, 2005.

[18] Biosurfit, 8 January 2015. URL `http://biosurfit.com`.

[19] Biosurfit, 9 January 2015. URL `http://biosurfit.com/solution/#pipeline`.

[20] J. Ducrée, S. Haeberle, S. Lutz, S. Pausch, F. Von Stetten, and R. Zengerle. The centrifugal microfluidic bio-disk platform. *Journal of Micromechanics and Microengineering*, 17(7):S103, 2007.

[21] N. Ichikawa, K. Hosokawa, and R. Maeda. Interface motion of capillary-driven flow in rectangular microchannel. *Journal of colloid and interface science*, 280(1):155–164, 2004.

[22] M. Grumann. Readout of diagnostic assays on a centrifugal microfluidic platform. *Universitat Freiburg im Breisgau*, 2005.

[23] C.-C. Hong, J.-W. Choi, and C. H. Ahn. A novel in-plane passive microfluidic mixer with modified tesla structures. *Lab on a Chip*, 4(2):109–113, 2004.

[24] B. Dabkowski. Coagulation analysers - point of care, self monitoring. *CAP Today*, pages 12 – 22, May 2013.

[25] J. Steigert, M. Grumann, T. Brenner, L. Riegger, J. Harter, R. Zengerle, and J. Ducrée. Fully integrated whole blood testing by real-time absorption measurement on a centrifugal platform. *Lab on a Chip*, 6(8):1040–1044, 2006.

[26] C. Hancher, L. Thacker, and E. Phares. A fiber-optic retroreflective turbidimeter for continuously monitoring cell concentration during fermentation. *Biotechnology and bioengineering*, 16(4):475–484, 1974.

[27] J. Steigert, M. Grumann, M. Dube, W. Streule, L. Riegger, T. Brenner, P. Koltay, K. Mittmann, R. Zengerle, and J. Ducrée. Direct hemoglobin measurement on a centrifugal microfluidic platform for point-of-care diagnostics. *Sensors and Actuators A: Physical*, 130:228–233, 2006.

[28] Ł. Tymecki, M. Pokrzywnicka, and R. Koncki. Paired emitter detector diode (pedd)-based photometry–an alternative approach. *Analyst*, 133(11):1501–1504, 2008.

[29] E. Mieczkowska, R. Koncki, and Ł. Tymecki. Hemoglobin determination with paired emitter detector diode. *Analytical and bioanalytical chemistry*, 399(9):3293–3297, 2011.

[30] F. Thomaz. *spinit*® clinical chemistry assay, master thesis. *Instituto Superior Técnico*, 2014.

[31] R. Gorkin, M. Czugala, C. Rovira-Borras, J. Ducree, D. Diamond, and F. Benito-Lopez. A wireless paired emitter detector diode device as an optical sensor for lab-on-a-disc applications. In *Solid-State Sensors, Actuators and Microsystems Conference (TRANSDUCERS), 2011 16th International*, pages 2526–2529. IEEE, 2011.

[32] K.-T. Lau, S. Baldwin, M. Ooole, R. Shepherd, W. J. Yerazunis, S. Izuo, S. Ueyama, and D. Diamond. A low-cost optical sensing device based on paired emitter–detector light emitting diodes. *Analytica Chimica Acta*, 557(1):111–116, 2006.

[33] K.-T. Lau, S. Baldwin, E. McHugh, and D. Diamond. Paired emitter-detector light emitting diodes for the measurement of lead(ii) and cadmium(ii=. *Analytica Chimica Acta*, 569:221–226, 2006.